Available online at www.sciencedirect.com
SCIENCE DIRECT®
Nuclear Physics B 695 (2004) 3–37
NUCLEAR PHYSICS B
www.elsevier.com/locate/npe

Exclusive electroproduction of J/ψ mesons at HERA

ZEUS Collaboration

S. Chekanov, M. Derrick, J.H. Loizides [1], S. Magill, S. Miglioranzi [1], B. Musgrave, J. Repond, R. Yoshida

Argonne National Laboratory, Argonne, IL 60439-4815, USA [40]

M.C.K. Mattingly

Andrews University, Berrien Springs, MI 49104-0380, USA

N. Pavel

Institut für Physik der Humboldt-Universität zu Berlin, Berlin, Germany

P. Antonioli, G. Bari, M. Basile, L. Bellagamba, D. Boscherini, A. Bruni, G. Bruni, G. Cara Romeo, L. Cifarelli, F. Cindolo, A. Contin, M. Corradi, S. De Pasquale, P. Giusti, G. Iacobucci, A. Margotti, A. Montanari, R. Nania, F. Palmonari, A. Pesci, L. Rinaldi, G. Sartorelli, A. Zichichi

University and INFN Bologna, Bologna, Italy [31]

G. Aghuzumtsyan, D. Bartsch, I. Brock, S. Goers, H. Hartmann, E. Hilger, P. Irrgang, H.-P. Jakob, O. Kind, U. Meyer, E. Paul [2], J. Rautenberg, R. Renner, A. Stifutkin, J. Tandler [3], K.C. Voss, M. Wang

Physikalisches Institut der Universität Bonn, Bonn, Germany [28]

D.S. Bailey [4], N.H. Brook, J.E. Cole, G.P. Heath, T. Namsoo, S. Robins, M. Wing

H.H. Wills Physics Laboratory, University of Bristol, Bristol, United Kingdom [39]

0550-3213/$ – see front matter
doi:10.1016/j.nuclphysb.2004.06.034

RAPID COMMUNICATION

M. Capua, A. Mastroberardino, M. Schioppa, G. Susinno

Calabria University, Physics Department and INFN, Cosenza, Italy [31]

J.Y. Kim, I.T. Lim, K.J. Ma, M.Y. Pac [5]

Chonnam National University, Kwangju, South Korea [33]

M. Helbich, Y. Ning, Z. Ren, W.B. Schmidke, F. Sciulli

Nevis Laboratories, Columbia University, Irvington on Hudson, NY 10027, USA [41]

J. Chwastowski, A. Eskreys, J. Figiel, A. Galas, K. Olkiewicz, P. Stopa, L. Zawiejski

Institute of Nuclear Physics, Cracow, Poland [35]

L. Adamczyk, T. Bołd, I. Grabowska-Bołd [6], D. Kisielewska, A.M. Kowal, M. Kowal, J. Łukasik, M. Przybycień, L. Suszycki, D. Szuba, J. Szuba [7]

Faculty of Physics and Nuclear Techniques, AGH-University of Science and Technology, Cracow, Poland [42]

A. Kotański [8], W. Słomiński

Department of Physics, Jagellonian University, Cracow, Poland

V. Adler, U. Behrens, I. Bloch, K. Borras, V. Chiochia, D. Dannheim [9], G. Drews, J. Fourletova, U. Fricke, A. Geiser, P. Göttlicher [10], O. Gutsche, T. Haas, W. Hain, S. Hillert [11], C. Horn, B. Kahle, U. Kötz, H. Kowalski, G. Kramberger, H. Labes, D. Lelas, H. Lim, B. Löhr, R. Mankel, I.-A. Melzer-Pellmann, C.N. Nguyen, D. Notz, A.E. Nuncio-Quiroz, A. Polini, A. Raval, L. Rurua, U. Schneekloth, U. Stösslein, G. Wolf, C. Youngman, W. Zeuner

Deutsches Elektronen-Synchrotron DESY, Hamburg, Germany

S. Schlenstedt

DESY Zeuthen, Zeuthen, Germany

G. Barbagli, E. Gallo, C. Genta, P.G. Pelfer

University and INFN, Florence, Italy [31]

A. Bamberger, A. Benen, F. Karstens, D. Dobur, N.N. Vlasov

Fakultät für Physik der Universität Freiburg i.Br., Freiburg i.Br., Germany [28]

M. Bell, P.J. Bussey, A.T. Doyle, J. Ferrando, J. Hamilton, S. Hanlon, D.H. Saxon, I.O. Skillicorn

Department of Physics and Astronomy, University of Glasgow, Glasgow, United Kingdom [39]

I. Gialas

Department of Engineering in Management and Finance, University of Aegean, Greece

T. Carli, T. Gosau, U. Holm, N. Krumnack, E. Lohrmann, M. Milite, H. Salehi, P. Schleper, T. Schörner-Sadenius, S. Stonjek [11], K. Wichmann, K. Wick, A. Ziegler, Ar. Ziegler

Hamburg University, Institute of Experimental Physics, Hamburg, Germany [28]

C. Collins-Tooth, C. Foudas, R. Gonçalo [12], K.R. Long, A.D. Tapper

Imperial College London, High Energy Nuclear Physics Group, London, United Kingdom [39]

P. Cloth, D. Filges

Forschungszentrum Jülich, Institut für Kernphysik, Jülich, Germany

M. Kataoka [13], K. Nagano, K. Tokushuku [14], S. Yamada, Y. Yamazaki

Institute of Particle and Nuclear Studies, KEK, Tsukuba, Japan [32]

A.N. Barakbaev, E.G. Boos, N.S. Pokrovskiy, B.O. Zhautykov

Institute of Physics and Technology of Ministry of Education and Science of Kazakhstan, Almaty, Kazakhstan

D. Son

Kyungpook National University, Center for High Energy Physics, Daegu, South Korea [33]

K. Piotrzkowski

Institut de Physique Nucléaire, Université Catholique de Louvain, Louvain-la-Neuve, Belgium

F. Barreiro, C. Glasman [15], O. González, L. Labarga, J. del Peso,
E. Tassi, J. Terrón, M. Zambrana

Departamento de Física Teórica, Universidad Autónoma de Madrid, Madrid, Spain [38]

M. Barbi, F. Corriveau, S. Gliga, J. Lainesse, S. Padhi, D.G. Stairs,
R. Walsh

Department of Physics, McGill University, Montréal, PQ, H3A 2T8 Canada [27]

T. Tsurugai

Meiji Gakuin University, Faculty of General Education, Yokohama, Japan [32]

A. Antonov, P. Danilov, B.A. Dolgoshein, D. Gladkov,
V. Sosnovtsev, S. Suchkov

Moscow Engineering Physics Institute, Moscow, Russia [36]

R.K. Dementiev, P.F. Ermolov, I.I. Katkov, L.A. Khein,
I.A. Korzhavina, V.A. Kuzmin, B.B. Levchenko, O.Yu. Lukina,
A.S. Proskuryakov, L.M. Shcheglova, S.A. Zotkin

Moscow State University, Institute of Nuclear Physics, Moscow, Russia [37]

I. Abt, C. Büttner, A. Caldwell, X. Liu, J. Sutiak

Max-Planck-Institut für Physik, München, Germany

N. Coppola, S. Grijpink, E. Koffeman, P. Kooijman, E. Maddox,
A. Pellegrino, S. Schagen, H. Tiecke, M. Vázquez, L. Wiggers,
E. de Wolf

NIKHEF and University of Amsterdam, Amsterdam, Netherlands [34]

N. Brümmer, B. Bylsma, L.S. Durkin, T.Y. Ling

Physics Department, Ohio State University, Columbus, OH 43210, USA [40]

A.M. Cooper-Sarkar, A. Cottrell, R.C.E. Devenish, B. Foster,
G. Grzelak, C. Gwenlan [16], T. Kohno, S. Patel, P.B. Straub,
R. Walczak

Department of Physics, University of Oxford, Oxford, United Kingdom [39]

A. Bertolin, R. Brugnera, R. Carlin, F. Dal Corso, S. Dusini, A. Garfagnini, S. Limentani, A. Longhin, A. Parenti, M. Posocco, L. Stanco, M. Turcato

Dipartimento di Fisica dell' Università and INFN, Padova, Italy [31]

E.A. Heaphy, F. Metlica, B.Y. Oh, J.J. Whitmore [17]

Department of Physics, Pennsylvania State University, University Park, PA 16802, USA [41]

Y. Iga

Polytechnic University, Sagamihara, Japan [32]

G. D'Agostini, G. Marini, A. Nigro

Dipartimento di Fisica, Università 'La Sapienza' and INFN, Rome, Italy [31]

C. Cormack [18], J.C. Hart, N.A. McCubbin

Rutherford Appleton Laboratory, Chilton, Didcot, Oxon, United Kingdom [39]

C. Heusch

University of California, Santa Cruz, CA 95064, USA [40]

I.H. Park

Department of Physics, Ewha Womans University, Seoul, South Korea

H. Abramowicz, A. Gabareen, S. Kananov, A. Kreisel, A. Levy

Raymond and Beverly Sackler Faculty of Exact Sciences, School of Physics, Tel-Aviv University, Tel-Aviv, Israel [30]

M. Kuze

Department of Physics, Tokyo Institute of Technology, Tokyo, Japan [32]

T. Fusayasu, S. Kagawa, T. Tawara, T. Yamashita

Department of Physics, University of Tokyo, Tokyo, Japan [32]

R. Hamatsu, T. Hirose [2], M. Inuzuka, H. Kaji, S. Kitamura [19], K. Matsuzawa

Tokyo Metropolitan University, Department of Physics, Tokyo, Japan [32]

M. Costa, M.I. Ferrero, V. Monaco, R. Sacchi, A. Solano

Università di Torino and INFN, Torino, Italy [31]

M. Arneodo, M. Ruspa

Università del Piemonte Orientale, Novara, and INFN, Torino, Italy [31]

T. Koop, J.F. Martin, A. Mirea

Department of Physics, University of Toronto, Toronto, ON, M5S 1A7 Canada [27]

J.M. Butterworth [20], R. Hall-Wilton, T.W. Jones, M.S. Lightwood, M.R. Sutton [4], C. Targett-Adams

Physics and Astronomy Department, University College London, London, United Kingdom [39]

J. Ciborowski [21], R. Ciesielski [22], P. Łużniak [23], R.J. Nowak, J.M. Pawlak, J. Sztuk [24], T. Tymieniecka, A. Ukleja, J. Ukleja [25], A.F. Żarnecki

Warsaw University, Institute of Experimental Physics, Warsaw, Poland [43]

M. Adamus, P. Plucinski

Institute for Nuclear Studies, Warsaw, Poland [43]

Y. Eisenberg, D. Hochman, U. Karshon, M. Riveline

Department of Particle Physics, Weizmann Institute, Rehovot, Israel [29]

A. Everett, L.K. Gladilin [26], D. Kçira, S. Lammers, L. Li, D.D. Reeder, M. Rosin, P. Ryan, A.A. Savin, W.H. Smith

Department of Physics, University of Wisconsin, Madison, WI 53706, USA [40]

S. Dhawan

Department of Physics, Yale University, New Haven, CT 06520-8121, USA [40]

S. Bhadra, C.D. Catterall, S. Fourletov, G. Hartner, S. Menary, M. Soares, J. Standage

Department of Physics, York University, Ontario, M3J 1P3 Canada [27]

Received 2 June 2004; accepted 11 June 2004

E-mail address: yoshida@mail.desy.de (R. Yoshida).

[1] Also affiliated with University College London, London, UK.

[2] Retired.

[3] Self-employed.

[4] PPARC Advanced Fellow.

[5] Now at Dongshin University, Naju, South Korea.

[6] Partly supported by Polish Ministry of Scientific Research and Information Technology, grant No. 2P03B 12225.

[7] Partly supported by Polish Ministry of Scientific Research and Information Technology, grant No. 2P03B 12625.

[8] Supported by the Polish State Committee for Scientific Research, grant No. 2P03B 09322.

[9] Now at Columbia University, NY, USA.

[10] Now at DESY group FEB.

[11] Now at University of Oxford, Oxford, UK.

[12] Now at Royal Holoway University of London, London, UK.

[13] Also at Nara Women's University, Nara, Japan.

[14] Also at University of Tokyo, Tokyo, Japan.

[15] Ramón y Cajal Fellow.

[16] PPARC Postdoctoral Research Fellow.

[17] On leave of absence at The National Science Foundation, Arlington, VA, USA.

[18] Now at University of London, Queen Mary College, London, UK.

[19] Present address: Tokyo Metropolitan University of Health Sciences, Tokyo 116-8551, Japan.

[20] Also at University of Hamburg, Alexander von Humboldt Fellow.

[21] Also at Łódź University, Poland.

[22] Supported by the Polish State Committee for Scientific Research, grant No. 2P03B 07222.

[23] Łódź University, Poland.

[24] Łódź University, Poland, supported by the KBN grant No. 2P03B 12925.

[25] Supported by the KBN grant No. 2P03B 12725.

[26] On leave from MSU, partly supported by the Weizmann Institute via the US–Israel BSF.

[27] Supported by the Natural Sciences and Engineering Research Council of Canada (NSERC).

[28] Supported by the German Federal Ministry for Education and Research (BMBF), under contract Nos. HZ1GUA 2, HZ1GUB 0, HZ1PDA 5, HZ1VFA 5.

[29] Supported by the MINERVA Gesellschaft für Forschung GmbH, the Israel Science Foundation, the US–Israel Binational Science Foundation and the Benozyio Center for High Energy Physics.

[30] Supported by the German–Israeli Foundation and the Israel Science Foundation.

[31] Supported by the Italian National Institute for Nuclear Physics (INFN).

[32] Supported by the Japanese Ministry of Education, Culture, Sports, Science and Technology (MEXT) and its grants for Scientific Research.

[33] Supported by the Korean Ministry of Education and Korea Science and Engineering Foundation.

[34] Supported by the Netherlands Foundation for Research on Matter (FOM).

[35] Supported by the Polish State Committee for Scientific Research, grant No. 620/E-77/SPB/DESY/P-03/DZ117/2003-2005.

[36] Partially supported by the German Federal Ministry for Education and Research (BMBF).

[37] Supported by RF President grant No. 1685.2003.2 for the leading scientific schools and by the Russian Ministry of Industry, Science and Technology through its grant for Scientific Research on High Energy Physics.

[38] Supported by the Spanish Ministry of Education and Science through funds provided by CICYT.

[39] Supported by the Particle Physics and Astronomy Research Council, UK.

[40] Supported by the US Department of Energy.

[41] Supported by the US National Science Foundation.

Abstract

The exclusive electroproduction of J/ψ mesons, $ep \to epJ/\psi$, has been studied with the ZEUS detector at HERA for virtualities of the exchanged photon in the ranges $0.15 < Q^2 < 0.8\ \mathrm{GeV}^2$ and $2 < Q^2 < 100\ \mathrm{GeV}^2$ using integrated luminosities of 69 and 83 pb^{-1}, respectively. The photon–proton centre-of-mass energy was in the range $30 < W < 220$ GeV and the squared four-momentum transfer at the proton vertex $|t| < 1\ \mathrm{GeV}^2$. The cross sections and decay angular distributions are presented as functions of Q^2, W and t. The effective parameters of the pomeron trajectory are in agreement with those found in J/ψ photoproduction. The spin-density matrix elements, calculated from the decay angular distributions, are consistent with the hypothesis of s-channel helicity conservation. The ratio of the longitudinal to transverse cross sections, σ_L/σ_T, grows with Q^2, whilst no dependence on W or t is observed. The results are in agreement with perturbative QCD calculations and exhibit a strong sensitivity to the gluon distribution in the proton.

1. Introduction

The exclusive electroproduction of light (ρ, ω, ϕ) and heavy ($J/\psi, \psi', \Upsilon$) vector mesons, $ep \to eVp$, has been investigated at HERA [1–9]. The increased precision of the recent data allows the study of the dependence of this process on the different scales involved: the mass squared of the vector meson, M_V^2, the square of the centre-of-mass energy of the photon–proton system, W^2, the exchanged-photon virtuality, Q^2, and the four-momentum transfer squared at the proton vertex, t.

Exclusive electroproduction of vector mesons involving a sufficiently large scale is calculable perturbatively because of the QCD factorisation theorem [10]. QCD-based models of this process assume that the exchanged virtual photon, seen from the proton rest-frame, fluctuates into a quark–antiquark pair which interacts with the proton via the exchange of two gluons in a colour-singlet configuration. After the interaction, the $q\bar{q}$ pair becomes a bound state. The cross section is proportional to the generalised parton distribution functions (GPDs) [11–13] of the proton, which contain information on the momentum distributions of the partons in the proton and their correlations. At the leading-order approximation in $\ln(1/x)$ and vanishing t, the generalised gluon distribution can be approximated by the usual gluon distribution. The gluon density is probed at $x \simeq (Q^2 + M_V^2)/W^2$ and at a scale $\mu^2 \simeq Q^2 + M_V^2$ [14]. The cross section is thus expected to rise steeply with W, a reflection of the steep rise of the gluon density as x decreases.

Data from exclusive ρ production [1–3] show that the cross section $\sigma(\gamma^* p \to \rho p)$ rises with W as W^δ, with δ increasing with Q^2 from about 0.2 at $Q^2 = 0$ (photoproduction) to about 0.8 at $Q^2 \approx 30\ \mathrm{GeV}^2$. However, in the case of exclusive J/ψ production the cross

[42] Supported by the Polish Ministry of Scientific Research and Information Technology, grant No. 112/E-356/SPUB/DESY/P-03/DZ116/2003-2005.

[43] Supported by the Polish State Committee for Scientific Research, grant No. 115/E-343/SPUB-M/DESY/P-03/DZ121/2001-2002, 2P03B 07022.

section rises steeply with W even for photoproduction [9]. It is therefore interesting to investigate J/ψ production at larger values of Q^2.

This paper presents measurements of the exclusive electroproduction of J/ψ mesons. Cross sections are given as functions of W, Q^2 and t. The W dependence is also studied as a function of t. The helicity structure of the J/ψ has been investigated to test s-channel helicity conservation (SCHC) and to extract the ratio of the cross sections for longitudinally (σ_L) and transversely (σ_T) polarised virtual photons, $R = \sigma_L/\sigma_T$, as a function of W, Q^2 and t. The results are compared to perturbative QCD (pQCD) model calculations.

The data cover the kinematic range $30 < W < 220$ GeV and $|t| < 1\ \text{GeV}^2$ for two ranges of photon virtuality: $0.15 < Q^2 < 0.8\ \text{GeV}^2$ (low-Q^2 sample) and $2 < Q^2 < 100\ \text{GeV}^2$ (high-Q^2 sample). The low-Q^2 sample was measured in the e^+e^- decay channel and the high-Q^2 sample in both e^+e^- and $\mu^+\mu^-$ channels. The low-Q^2 range has been measured for the first time. The high-Q^2 sample represents more than an order of magnitude increase in statistics compared to the previous ZEUS results [1], and extends both the W and Q^2 ranges of the measurement.

2. Experimental set-up

The data used for this measurement were taken at the HERA ep collider using the ZEUS detector in 1998–2000. During this period, HERA operated with a proton energy of 920 GeV and an electron[44] energy of 27.5 GeV. The data correspond to integrated luminosities of 69 pb^{-1} for the low-Q^2 sample and 83 pb^{-1} for the high-Q^2 sample.

A detailed description of the ZEUS detector can be found elsewhere [15]. A brief outline of the components that are most relevant for this analysis is given below.

Charged particles were reconstructed in the central tracking detector (CTD) [16–18] covering the polar-angle[45] region $15° < \theta < 164°$. The transverse-momentum resolution for full-length tracks is $\sigma(p_T)/p_T = 0.0058 p_T \oplus 0.0065 \oplus 0.0014/p_T$, with p_T in GeV.

The high-resolution uranium-calorimeter (CAL) [19–22] consists of three parts: the forward (FCAL), the barrel (BCAL) and the rear (RCAL) calorimeters. Each part is subdivided transversely into towers and longitudinally into an electromagnetic section (EMC) and either one (RCAL) or two (FCAL and BCAL) hadronic sections. The CAL covers 99.7% of the total solid angle. The energy resolution obtained from test-beam measurements was $\sigma(E)/E = 0.18/\sqrt{E}$ in the electromagnetic sections and $\sigma(E)/E = 0.35/\sqrt{E}$ in the hadronic sections, with E in GeV.

The forward plug calorimeter (FPC) [23] was a lead-scintillator sandwich calorimeter with readout via wavelength shifter fibres. It was installed in the beamhole of the FCAL and extended the pseudorapidity coverage of the forward calorimeter from $\eta \lesssim 4$ to $\eta \lesssim 5$.

The beampipe calorimeter (BPC) [24] was a tungsten-scintillator sampling calorimeter installed to measure scattered electrons at small angles, in the range $1.15° < 180° - \theta <$

[44] Hereafter, both e^+ and e^- are referred to as electrons, unless explicitly stated otherwise.

[45] The ZEUS coordinate system is a right-handed Cartesian system, with the Z axis pointing in the proton beam direction, referred to as the "forward direction", and the X axis pointing left towards the centre of HERA. The coordinate origin is at the nominal interaction point.

2.30°. The energy resolution, as measured under test-beam conditions, was $\sigma(E)/E = 0.17/\sqrt{E}$, with E in GeV. The impact position of the scattered electron was measured with an accuracy of about 0.5 mm corresponding to an angular resolution of 0.17 mrad.

The small-angle rear tracking detector (SRTD) [25] consists of two planes of scintillator strips read out via optical fibres and photomultiplier tubes. It is attached to the front face of the RCAL and covers an angular range between 4° and 18° around the beampipe. The SRTD provides a transverse position resolution of 0.3 cm [9] corresponding to an angular resolution of 2 mrad.

The hadron–electron separator installed in the RCAL (RHES) [15] consists of silicon diodes placed at a longitudinal depth of three radiation lengths. The RHES provides an electron position resolution of 0.9 cm for a single hit and 0.5 cm if the shower spans at least two adjacent pads [26].

The luminosity was determined from the rate of the bremsstrahlung process $ep \to e\gamma p$, where the photon was measured with a lead-scintillator calorimeter [27] located at $Z = -107$ m in the HERA tunnel.

3. Kinematics and cross sections

The following kinematic variables are used to describe exclusive J/ψ production, $e(k)p(P) \to e(k')J/\psi(v)p(P')$, where k, k', P, P' and v are, respectively, the four-momenta of the incident electron, scattered electron, incident proton, scattered proton and J/ψ:

- $Q^2 = -q^2 = -(k - k')^2$, the negative four-momentum squared of the virtual photon;
- $W^2 = (q + P)^2$, the squared invariant mass of the photon–proton system;
- $y = (P \cdot q)/(P \cdot k)$, the fraction of the electron energy transferred to the proton in the proton rest frame;
- $x = Q^2/(2P \cdot q)$, the Bjorken variable;
- $t = (P - P')^2$, the squared four-momentum transfer at the proton vertex.

The kinematic variables were reconstructed with the "constrained" method [1] which uses the momentum of the J/ψ and the polar and azimuthal angles of the scattered electron.

The ep cross section can be expressed in terms of the transverse, σ_T, and longitudinal, σ_L, virtual photoproduction cross sections as

$$\frac{d^2\sigma^{ep\to eJ/\psi p}}{dy\,dQ^2} = \Gamma_T\left(y, Q^2\right)(\sigma_T + \epsilon\sigma_L),$$

where Γ_T is the flux of transverse virtual photons [28] and ϵ is the ratio of longitudinal and transverse virtual photon fluxes, given by $\epsilon = 2(1 - y)/(1 + (1 - y)^2)$. In the kinematic range studied here, ϵ is in the range $0.8 < \epsilon < 1$, with an average value of 0.99.

The virtual photon–proton cross section, $\sigma^{\gamma^* p \to J/\psi p} \equiv \sigma_T + \epsilon \sigma_L$, can be used to evaluate the total exclusive cross section, $\sigma_{\text{tot}}^{\gamma^* p \to J/\psi p} \equiv \sigma_T + \sigma_L$, through the relation

$$\sigma_{\text{tot}}^{\gamma^* p \to J/\psi p} = \frac{1+R}{1+\epsilon R} \sigma^{\gamma^* p \to J/\psi p},$$

where $R = \sigma_L/\sigma_T$ is the ratio of the cross sections for longitudinal and transverse photons. The helicity structure of the J/ψ production is used to determine R as described in Section 7.6.1.

4. Reconstruction and selection of the events

The signature of exclusive J/ψ electroproduction, $ep \to eJ/\psi p$, consists of the scattered electron and two charged leptons from the J/ψ decay, e^+e^- or $\mu^+\mu^-$. The scattered proton is deflected through a small angle and escapes undetected down the beampipe.

The events were selected online by a three-level trigger [29,30]. For the low-Q^2 sample, the trigger [9] for J/ψ photoproduction events with decay to the e^+e^- final state was used, while for the high-Q^2 sample, the trigger required a scattered electron in the CAL with energy greater than 4 GeV.

The following criteria were applied offline to reconstruct and select the events [31–33]:

- the energy and position of the scattered electron were measured in the BPC for the low-Q^2 sample and in the CAL for the high-Q^2 sample. The energy was required to satisfy $E_e > 10$ GeV. The position measurement of the CAL was improved using the SRTD (88% of the events) and the RHES (10% of the events). To ensure full containment of the electromagnetic shower, fiducial cuts were applied to the impact position of the electron on face of the RCAL;
- the J/ψ mesons were reconstructed from the decay leptons. Two tracks of opposite charge, well-reconstructed in the CTD with $p_T > 0.2$ GeV, were selected (two-track events). In the case of the electron decay channel, events were also selected by requiring one well-reconstructed CTD track and one CAL energy cluster [34] not related to the track (one-track events). In addition:
  - the two-track events were required to have the higher-momentum track matched to a calorimeter energy cluster for which the fraction of the energy deposited in the EMC was consistent with that of an electron or a muon;
  - the one-track events were accepted if, in addition to the measured CTD track associated with a CAL cluster, the second cluster lay in the angular range outside the CTD acceptance with energy between 2 and 10 GeV. Both clusters were required to have a fraction of energy deposited in the EMC consistent with that of an electron.

For both types of events, one additional CTD track was allowed. If present, this track was required to match the scattered electron. Events with further tracks were rejected:

- the position of the reconstructed vertex was required to be compatible with that of an ep collision;
- to remove events with large initial-state radiation and to reduce the background from photoproduction, the requirement $45 < \delta < 65$ GeV was imposed, where $\delta = \sum E_i(1 - \cos\theta_i)$, E_i is the energy of the ith calorimeter cell, θ_i its polar angle and the sum runs over the cells associated to the final-state leptons;
- to suppress non-exclusive events, the energy of each CAL cluster not associated to any of the final-state leptons was required to be less than 0.3 or 0.4 GeV, depending on the CAL section; these thresholds were set to be above the noise level of the CAL. To suppress further the contamination from proton-dissociative events, $ep \to eJ/\psi Y$, the energy in the FPC was required to be less than 1 GeV and the sum of the energy in the FCAL cells surrounding the beamhole to be less than 0.5 GeV. These cuts restrict the mass of the proton-dissociated system, Y, to $M_Y \lesssim 3.0$ GeV.

Unless otherwise stated, the results are quoted in the following kinematic range: $|t| < 1\ \text{GeV}^2$, $30 < W < 220$ GeV for the electron channel and $45 < W < 160$ GeV for the muon channel. The larger W range for the electron channel was achieved by the inclusion of the one-track events. The Q^2 range was $0.15 < Q^2 < 0.8\ \text{GeV}^2$ for the low-Q^2 sample and $2 < Q^2 < 100\ \text{GeV}^2$ for the high-Q^2 sample.

The final high-Q^2 sample contains 728 events in the muon channel and 955 events in the electron channel, 275 of which are reconstructed using only one track. The final low-Q^2 sample contains 137 events in the electron channel, 16 of which are reconstructed using only one track. The distribution of the events in the x–Q^2 plane is shown in Fig. 1.

5. Monte Carlo simulation

The acceptance and the effects of the detector response were determined using samples of Monte Carlo (MC) events. All generated events were passed through the standard ZEUS detector simulation, based on the GEANT 3.13 programme [35], and the ZEUS trigger simulation package.

The exclusive process $ep \to eJ/\psi p$ was modelled using the ZEUSVM [36] MC generator interfaced to HERACLES 4.6.1 [37,38] to account for first-order QED radiative effects. The $\gamma^* p \to J/\psi p$ cross section was parametrised as $W^\delta e^{-b|t|}(M^2_{J/\psi} + Q^2)^{-n}$. The parameter values $n = 2.5(2.3)$, $\delta = 0.75(0.7)$ and $b = 4.5(4.5)\ \text{GeV}^{-2}$ were used to describe the high-Q^2 (low-Q^2) data. The leptonic decay of the J/ψ was simulated by the PHOTOS programme [39] which includes final-state radiation from the decay leptons. This generator assumes SCHC and that the ratio of the cross sections for longitudinal and transverse photons is $R = 0.5(Q^2/M^2_{J/\psi})$.

Proton-dissociative events, $ep \to eJ/\psi Y$, were modelled using the generator EPSOFT [40,41]. The $\gamma^* p \to J/\psi Y$ cross section was parametrised as

$$\frac{d^2\sigma^{\gamma^* p \to J/\psi Y}}{dt\, dM^2} \propto W^\delta e^{-b|t|}\left(M^2_{J/\psi} + Q^2\right)^{-n} M_Y^{-\beta} \tag{1}$$

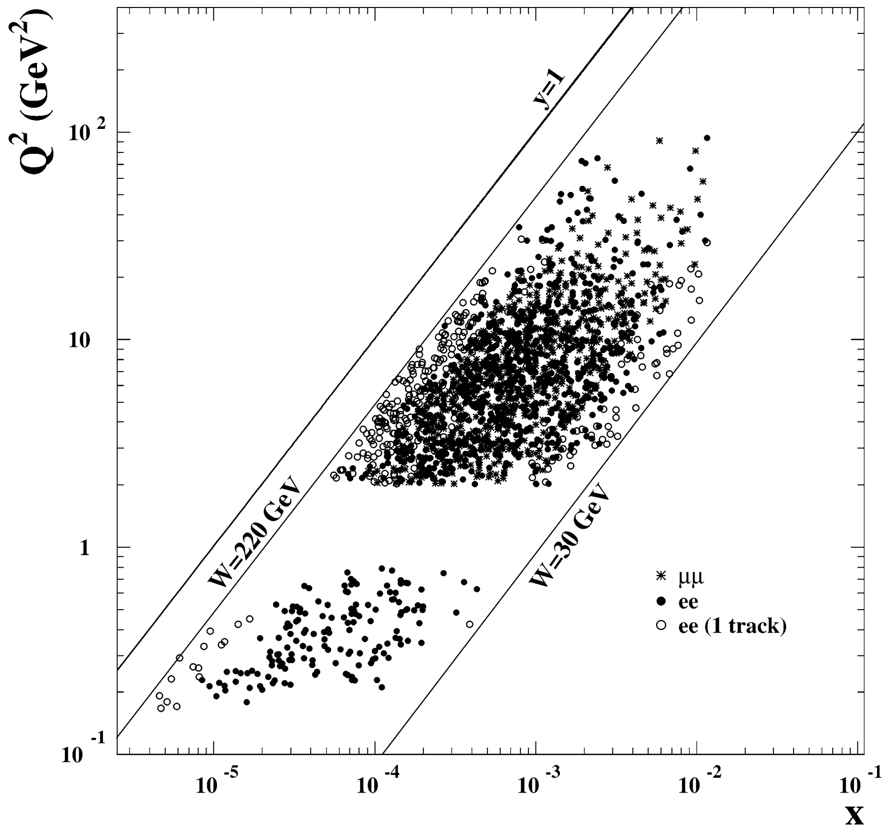

Fig. 1. The distribution of the events in the muon and electron channels in the kinematic plane of Bjorken-x and Q^2. The events reconstructed using one and two measured tracks are shown separately.

with the parameters $n = 2.5$, $\delta = 0.75$, $b = 0.81\ \text{GeV}^{-2}$ and $\beta = 2.57$ chosen as described in Section 6.2.

The QED background stemming from two-photon lepton-pair production $\gamma^*\gamma \to l^+l^-$, where the virtual photon originates from the electron vertex and the second photon is radiated off the proton, was simulated using the LPAIR [42] generator at low Q^2 and the GRAPE-DILEPTON 1.1 [43] generator at high Q^2. The QED-Compton-like processes with internal photon conversion were also generated with GRAPE.

6. Extraction of the J/ψ signal

Fig. 2 shows the invariant-mass distributions of the muon and electron pairs, obtained after the selection described in Section 4. The MC distributions for exclusive J/ψ production and the QED background are also shown. The width of the resonance is dominated by the detector resolution, which deteriorates at low and high values of W.

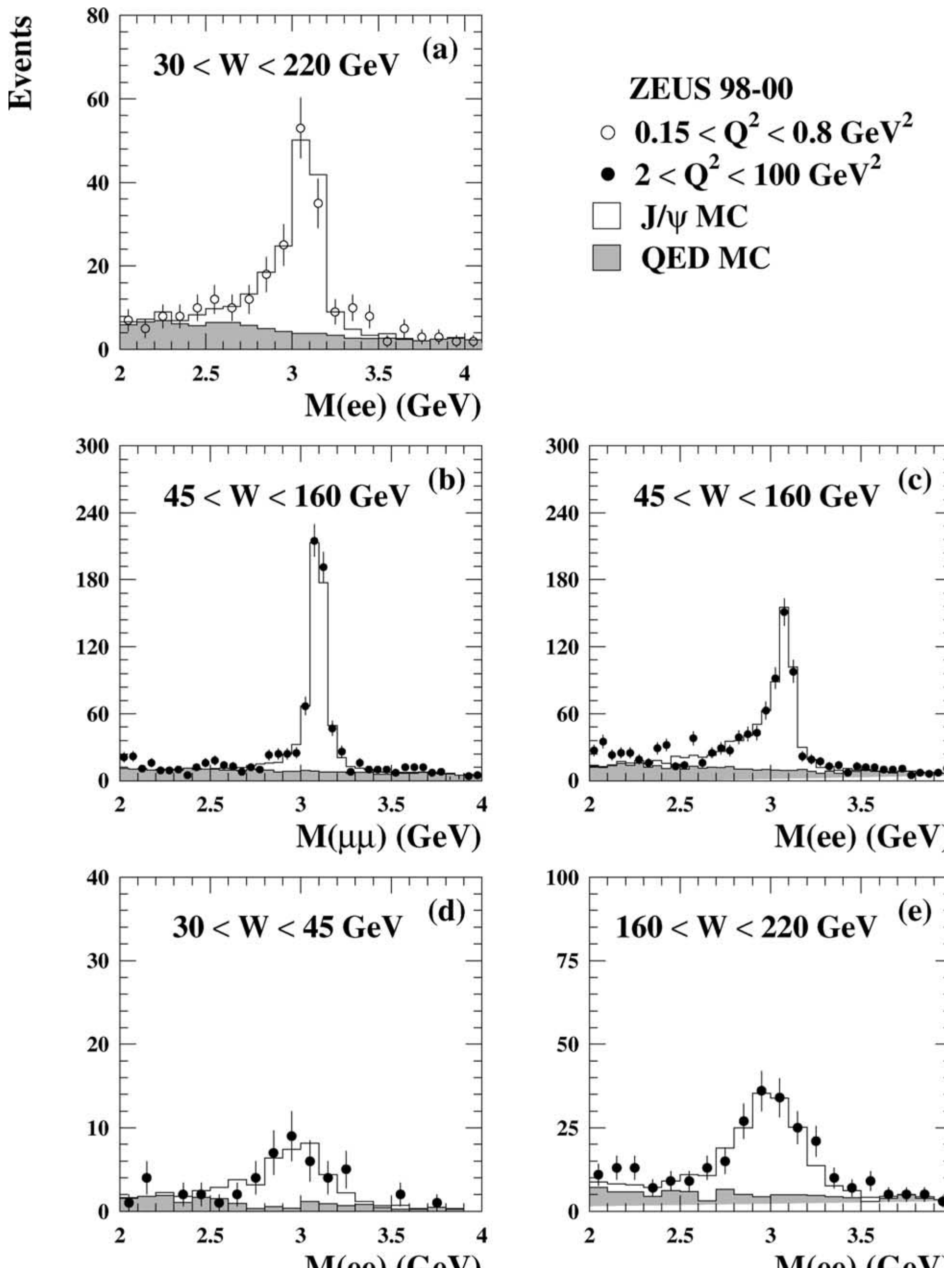

Fig. 2. Invariant mass distributions of the lepton pairs for (a) the low-Q^2 sample and (b)–(e) the high-Q^2 sample. The shaded histograms are the QED MC distributions and the open histograms the sum of the J/ψ and QED MC events. The small excess of data at low mass is due to background from pions. The error bars indicate the statistical uncertainties.

6.1. Non-resonant background

The non-resonant background was estimated from the MC distributions of the QED-background processes: two-photon lepton-pair production and Compton scattering. For the low-Q^2 sample, the normalisation of the QED-background was estimated from a two-parameter fit of the signal and the background MC distributions to the invariant mass spectra of the data. For the high-Q^2 sample, the normalisation was based on the known cross sections and the integrated luminosity of the data. After subtraction of the non-resonant distributions, the J/ψ signal was determined by counting the events in the mass windows $2.8 < M_{\mu^+\mu^-} < 3.4$ GeV for the muon channel and $2.6 < M_{e^+e^-} < 3.4$ GeV for the electron channel. The lower limit on $M_{e^+e^-}$ was chosen to include events with reduced invariant mass due to bremsstrahlung. The contribution of the non-resonant background in the signal range is typically 22% for the electron channel and 14% for the muon channel.

For the high-Q^2 sample, additional background from pions misidentified as electrons or muons was studied using a sample of events with two tracks, neither of which were identified as a muon or an electron. The contribution was $(2.7 \pm 0.6)\%$ for the electron channel and $(0.8 \pm 0.3)\%$ for the muon channel and was subtracted bin-by-bin for the t and decay-angle distributions and globally for the W and Q^2 distributions.

Events from exclusive $\psi(2S)$ production contribute to the J/ψ sample through two different decay channels: (i) $\psi(2S) \to J/\psi +$ neutrals (branching ratio $(23.9 \pm 1.2)\%$ [44]), where the neutrals are not detected in the CAL, and (ii) $\psi(2S) \to l^+l^-$ (branching ratios $(7.3 \pm 0.4) \times 10^{-3}$ for the electron channel and $(7.0 \pm 0.9) \times 10^{-3}$ for the muon decay channel [44]), because of the limited resolution in the reconstruction of the invariant mass. The contribution from both these processes to the J/ψ sample was determined using MC samples under the assumption that $\sigma(\psi(2S))/\sigma(J/\psi) = 0.166 \pm 0.013$ [8]. A contribution of $(1.8 \pm 0.2)\%$ was subtracted.

6.2. Proton-dissociative background

The remaining source of background consists of J/ψ production accompanied by proton dissociation, $ep \to eJ/\psi Y$, where the particles from the breakup of the proton are not detected.

Proton-dissociative events were studied using a sample of diffractive events selected as described in Section 4, with the following exceptions:

- the elasticity criterion (last criterion in Section 4) was not applied to the FPC and to a region of FCAL of approximately 50 cm radius around the beampipe;
- events with decay-lepton tracks at angles smaller than 30° with respect to the outgoing proton direction were removed to ensure a rapidity gap between the J/ψ and the system Y.

Proton-dissociative events were selected by requiring an energy larger than 1 GeV in the FPC. The sample of data tagged by the FPC contained 100 events for $|t| < 3\ \text{GeV}^2$ in the kinematic range $45 < W < 160$ GeV and $Q^2 > 2\ \text{GeV}^2$. The parameters (see Eq. (1)) that best describe the Q^2, W and t dependences are $n = 2.57 \pm 0.09$, $\delta = 0.61 \pm 0.40$

and $b = 0.81 \pm 0.25\ \mathrm{GeV}^{-2}$. The MC distribution of M_Y^2 was tuned to describe the FPC energy distribution, yielding $\beta = 2.57 \pm 0.67$. The values for n and δ are in agreement with those described in Section 7.3. The latter are more precise and were used in EPSOFT. The values of b and β are in agreement with those found for proton-dissociative J/ψ photoproduction [9].

The fraction of proton-dissociative events in the elastic sample, $f_{\text{p-diss}}$, was determined from the relation $f_{\text{p-diss}} = f_{\mathrm{FPC}}^{\mathrm{data}}(1/\epsilon' - 1)$, where $f_{\mathrm{FPC}}^{\mathrm{data}}$ denotes the fraction of the proton-dissociative sample tagged by the FPC and $\epsilon' = 32\%$ is the FPC tagging efficiency, estimated using EPSOFT. The fraction of proton-dissociative events in the final sample, averaged over t for $|t| < 1\ \mathrm{GeV}^2$, was $f_{\text{p-diss}} = (14.2 \pm 2.0(\text{stat.})^{+6.8}_{-3.6}(\text{syst.}))\%$, independent of W and Q^2. The systematic uncertainty was dominated by the uncertainty on β. The fraction increases from 4% for $0 < |t| < 0.1\ \mathrm{GeV}^2$ to 20% for $0.2 < |t| < 1.0\ \mathrm{GeV}^2$. The cross sections presented in the next sessions were corrected for this background in bins of t, and globally in W and Q^2.

7. Results

7.1. Measurement of cross sections

In each bin of a kinematic variable, the ep cross section was extracted for each decay channel using the formula

$$\sigma^{ep\to eJ/\psi p} = \frac{(N_{\mathrm{data}} - N_{\mathrm{bgd}})(1 - f_{p\text{-diss}})}{\mathcal{A}\mathcal{B}\mathcal{L}},$$

where N_{data} is the number of events in the data and N_{bgd} is the number of events from the non-resonant background (QED processes and pionic background) and $\psi(2S)$ production. The overall acceptance is denoted as $\mathcal{A}$, $\mathcal{B}$ accounts for the J/ψ decay branching ratios [44], $(5.93 \pm 0.10)\%$ and $(5.88 \pm 0.10)\%$ for the electron and muon channels, respectively, and $\mathcal{L}$ is the integrated luminosity.

The total exclusive photon–proton cross section was calculated as

$$\sigma_{\mathrm{tot}}^{\gamma^* p\to J/\psi p}(Q^2, W) = \big(1/\Phi(Q^2, W)\big)\frac{d^2\sigma^{ep\to eJ/\psi p}}{dQ^2\,dW},$$

where the effective photon flux Φ [45] contains the corrections for bin-centring and R, both estimated from the MC simulation. The final cross section was the error-weighted average of the cross sections for each decay channel.

The cross sections are quoted at the QED-Born level. The radiative corrections range from 1% to 10% (on average 5%), depending on the kinematic region.

The cross sections were measured for $|t| < 1\ \mathrm{GeV}^2$. Assuming $d\sigma/dt \propto e^{-b|t|}$, with $b = 4.5\ \mathrm{GeV}^{-2}$, the correction factor needed to extrapolate to the cross section integrated over the full t range is 1.012. In addition, for $x > 0.01$ both the acceptance and the expected cross section are small, and the measurement in this region therefore involves an extrapolation, made in order to quote the measurement in bins of W and Q^2. The uncertainty introduced by this extrapolation, as evaluated from the MC simulation, is negligible.

7.2. Systematic uncertainties

The systematic uncertainties on the measured cross sections were determined by varying the selection cuts and by modifying the analysis procedure. The sources of systematic uncertainties considered were similar to those of previously published analyses [9,46].

For the low-Q^2 sample, the main contribution arises from the uncertainty of ± 1 mm in the position of the BPC, leading to a $\pm 10\%$ uncertainty in the cross section.

For the high-Q^2 sample, the dominant sources of uncertainty are as follows. The corresponding average uncertainties are given in parentheses:

- the trigger efficiency ($^{+2.8}_{-1.2}\%$);
- the fiducial volume cut on the electron position was changed by ± 1 cm; the SRTD alignment was changed by ± 2 mm along the Y axis ($^{+5.5}_{-3.5}\%$). A maximum change of -11% was observed in the lowest Q^2 bin;
- the mass window used for signal extraction was extended by 0.1 GeV ($\pm 1.7\%$);
- the normalisation of the QED background was changed by $\pm 10\%$ ($\pm 2.4\%$); the maximum effect of $\pm 5\%$ was found for the lowest t bin.

The uncertainty due to the subtraction of proton-dissociative background has been discussed in Section 6.2. Additional contributions come from the uncertainties on the integrated luminosity, $\pm 2.25\%$, and on the branching ratios, $\pm 1.7\%$. Uncertainties from the minimum energy requirement of the scattered electron ($\pm 0.7\%$), the elasticity cut ($^{+0.2}_{-1.9}\%$), the selection of the electron and muon samples ($\pm 1.2\%$) and the dependence on the MC parametrisations ($\pm 0.7\%$) were also estimated. The total systematic uncertainty was determined by adding the individual contributions in quadrature. The correlated and uncorrelated systematic uncertainties were evaluated separately and were $^{+5}_{-8}\%$ and $^{+7.4}_{-6.4}\%$, respectively.

7.3. Dependence on W and Q^2

The cross section $\sigma_{\mathrm{tot}}^{\gamma^* p \to J/\psi p}$, measured as a function of W and Q^2 for $|t| < 1\ \mathrm{GeV}^2$, is given in Tables 1 and 2. The same cross section, extrapolated to the full t range, is shown in Fig. 3 together with the H1 [5] measurements[46] as well as the ZEUS measurement of exclusive J/ψ photoproduction [9]. The H1 measurements are systematically lower than the ZEUS data; however they are compatible when the normalisation uncertainties of both measurements are considered.

The functional form $\sigma \propto W^{\delta}$ was fitted to the ZEUS data; the results of the fit are shown in Fig. 3(a) and in Table 4. No significant variation of δ with Q^2 is seen. The mean value of δ is $0.73 \pm 0.11(\mathrm{stat.})^{+0.04}_{-0.08}(\mathrm{syst.})$. It is consistent with the values found for J/ψ photoproduction [1] and for ρ electroproduction at high Q^2 [2].

[46] In Fig. 3(a), the H1 cross sections, measured at Q^2 values of 3.5, 10.1 and 33.6 GeV^2, have been rescaled to the Q^2 values of 3.1, 6.8 and 16 GeV^2 using the Q^2 dependence of the data measured by H1. The systematic uncertainties due to this extrapolation were negligible.

Table 1
The cross sections for the reaction $\gamma^* p \to J/\psi p$ measured as a function of W in bins of Q^2 and for $|t| < 1\ \mathrm{GeV}^2$: $\langle W \rangle$ and $\langle Q^2 \rangle$ are the mean values in the indicated ranges; N_{ee} and $N_{\mu\mu}$ are the number of events in the signal region after non-resonant background subtraction of the electron and muon pairs, respectively; $\mathcal{A}_{ee}$ and $\mathcal{A}_{\mu\mu}$ are the corresponding acceptances. The first uncertainty of the cross sections is statistical and the second systematic. An overall normalisation uncertainty of $^{+5\%}_{-8\%}$ was not included

Q^2 (GeV^2)	$\langle Q^2 \rangle$ (GeV^2)	W (GeV)	$\langle W \rangle$ (GeV)	N_{ee}	$N_{\mu\mu}$	$\mathcal{A}_{ee}$	$\mathcal{A}_{\mu\mu}$	$\sigma^{ep\to J/\psi p}$ (pb)	$\sigma_{\mathrm{tot}}^{\gamma^* p\to J/\psi p}$ (nb)
0.15–0.8	0.4	30–65	49	32		0.031		$217 \pm 53^{+12}_{-19}$	$39.2 \pm 9.6^{+2.2}_{-3.4}$
		65–105	86	55		0.044		$257 \pm 46^{+18}_{-17}$	$75.7 \pm 13.5^{+5.2}_{-4.9}$
		105–220	167	50		0.021		$498 \pm 89^{+37}_{-38}$	$118.0 \pm 21.0^{+8.8}_{-9.1}$
2–5	3.1	30–45	37	29.2		0.111		$41.5 \pm 8.4^{+5.6}_{-6.6}$	$24.8 \pm 5.0^{+3.3}_{-3.9}$
		45–70	57	51.5	53.2	0.180	0.173	$48.8 \pm 5.2^{+3.1}_{-3.9}$	$27.4 \pm 3.0^{+1.8}_{-2.2}$
		70–90	80	36.7	60.0	0.204	0.224	$36.4 \pm 4.1^{+10.5}_{-3.0}$	$36.7 \pm 4.2^{+10.6}_{-3.0}$
		90–112	101	61.7	37.5	0.221	0.223	$35.4 \pm 4.0^{+3.0}_{-4.5}$	$43.0 \pm 4.8^{+3.7}_{-5.4}$
		112–145	128	51.2	46.4	0.197	0.167	$44.7 \pm 5.0^{+9.0}_{-4.3}$	$48.8 \pm 5.5^{+9.8}_{-4.7}$
		145–220	180	71.6		0.154		$76.5 \pm 10.3^{+11.5}_{-5.1}$	$61.1 \pm 8.2^{+9.2}_{-4.1}$
5–10	6.8	30–50	40	27.8		0.215		$19.6 \pm 4.1^{+3.9}_{-1.9}$	$12.7 \pm 2.7^{+2.5}_{-1.2}$
		50–74	62	48.7	45.8	0.403	0.383	$19.3 \pm 2.2^{+2.9}_{-1.3}$	$16.6 \pm 1.9^{+2.5}_{-1.1}$
		74–96	85	39.6	52.4	0.439	0.486	$15.6 \pm 1.8^{+1.6}_{-1.4}$	$20.7 \pm 2.3^{+2.2}_{-1.9}$
		96–120	108	37.1	46.4	0.479	0.514	$13.5 \pm 1.7^{+1.1}_{-0.7}$	$21.9 \pm 2.7^{+1.7}_{-1.2}$
		120–150	135	33.9	49.0	0.475	0.395	$14.9 \pm 1.9^{+1.1}_{-1.3}$	$25.8 \pm 3.3^{+1.9}_{-2.3}$
		150–220	183	58.4		0.343		$27.9 \pm 4.1^{+4.5}_{-1.4}$	$33.2 \pm 4.9^{+5.3}_{-1.6}$
10–100	16.0	30–55	42	16.1		0.235		$10.9 \pm 3.1^{+0.8}_{-1.0}$	$3.3 \pm 0.9^{+0.2}_{-0.3}$
		55–78	66	27.7	37.8	0.555	0.659	$8.4 \pm 1.2^{+1.4}_{-0.4}$	$4.5 \pm 0.6^{+0.7}_{-0.2}$
		78–100	89	31.0	43.6	0.673	0.728	$8.6 \pm 1.1^{+0.9}_{-1.4}$	$6.7 \pm 0.9^{+0.7}_{-1.1}$
		100–124	112	37.5	36.2	0.645	0.704	$8.4 \pm 1.1^{+0.4}_{-1.2}$	$7.9 \pm 1.0^{+0.3}_{-1.1}$
		124–160	141	39.6	41.3	0.563	0.591	$10.8 \pm 1.4^{+2.1}_{-0.8}$	$9.3 \pm 1.2^{+1.7}_{-0.7}$
		160–220	189	51.0		0.361		$25.1 \pm 3.8^{+1.7}_{-1.2}$	$20.8 \pm 3.1^{+1.4}_{-1.0}$

Table 2
The cross sections for the reaction $\gamma^* p \to J/\psi p$ measured as a function of Q^2, for a mean value $W = 90$ GeV and for $|t| < 1$ GeV^2: $\langle Q^2 \rangle$ indicates the mean value in the Q^2 range considered; N_{ee} and $N_{\mu\mu}$ are the numbers of events in the signal region after non-resonant background subtraction of the electron and muon pairs, respectively; $\mathcal{A}_{ee}$ and $\mathcal{A}_{\mu\mu}$ are the corresponding acceptances. The first uncertainty of the cross sections is statistical and the second systematic. An overall normalisation uncertainty of $^{+5\%}_{-8\%}$ was not included

Q^2 (GeV^2)	$\langle Q^2 \rangle$ (GeV^2)	N_{ee}	$\mathcal{A}_{ee}$	$\sigma_{ee}^{ep\to J/\psi p}$ (pb)	$N_{\mu\mu}$	$\mathcal{A}_{\mu\mu}$	$\sigma_{\mu\mu}^{ep\to J/\psi p}$ (pb)	$\sigma_{\text{tot}}^{\gamma^* p\to J/\psi p}$ (nb)
		ee: $30 < W < 220$ GeV			$\mu\mu$: $45 < W < 160$ GeV			$W = 90$ GeV
0.15–0.8	0.4	137.0	0.029	$954 \pm 108^{+63}_{-74}$				$72.6 \pm 8.2^{+4.8}_{-5.6}$
2–3.2	2.5	141.3	0.156	$150 \pm 14^{+53}_{-8}$	90.5	0.159	$96 \pm 11^{+5}_{-14}$	$39.7 \pm 2.9^{+5.9}_{-2.9}$
3.2–5	3.9	160.6	0.202	$132 \pm 12^{+8}_{-17}$	118.6	0.217	$91.6 \pm 8.9^{+12.2}_{-6.6}$	$38.7 \pm 2.5^{+3.3}_{-3.6}$
5–7	5.9	123.1	0.327	$59.9 \pm 6.1^{+5.5}_{-3.6}$	100.4	0.336	$48.7 \pm 5.2^{+1.2}_{-2.5}$	$24.3 \pm 1.8^{+1.1}_{-1.0}$
7–10	8.4	122.5	0.466	$42.6 \pm 4.3^{+4.7}_{-5.0}$	104.1	0.529	$32.5 \pm 3.4^{+4.4}_{-2.4}$	$15.8 \pm 1.2^{+1.5}_{-0.7}$
10–15	12	106.7	0.485	$36.7 \pm 4.0^{+1.4}_{-2.9}$	87.2	0.607	$24.1 \pm 2.8^{+1.2}_{-1.6}$	$11.6 \pm 1.0^{+0.4}_{-0.6}$
15–40	22	84.3	0.473	$29.3 \pm 3.7^{+2.0}_{-4.7}$	71.6	0.651	$18.4 \pm 2.4^{+0.9}_{-1.4}$	$4.0 \pm 0.4^{+0.2}_{-0.3}$
40–100	54	12.0	0.423	$4.5 \pm 1.5^{+0.5}_{-1.1}$	7.4	0.554	$2.2 \pm 0.9^{+0.4}_{-0.6}$	$0.65 \pm 0.17^{+0.08}_{-0.16}$

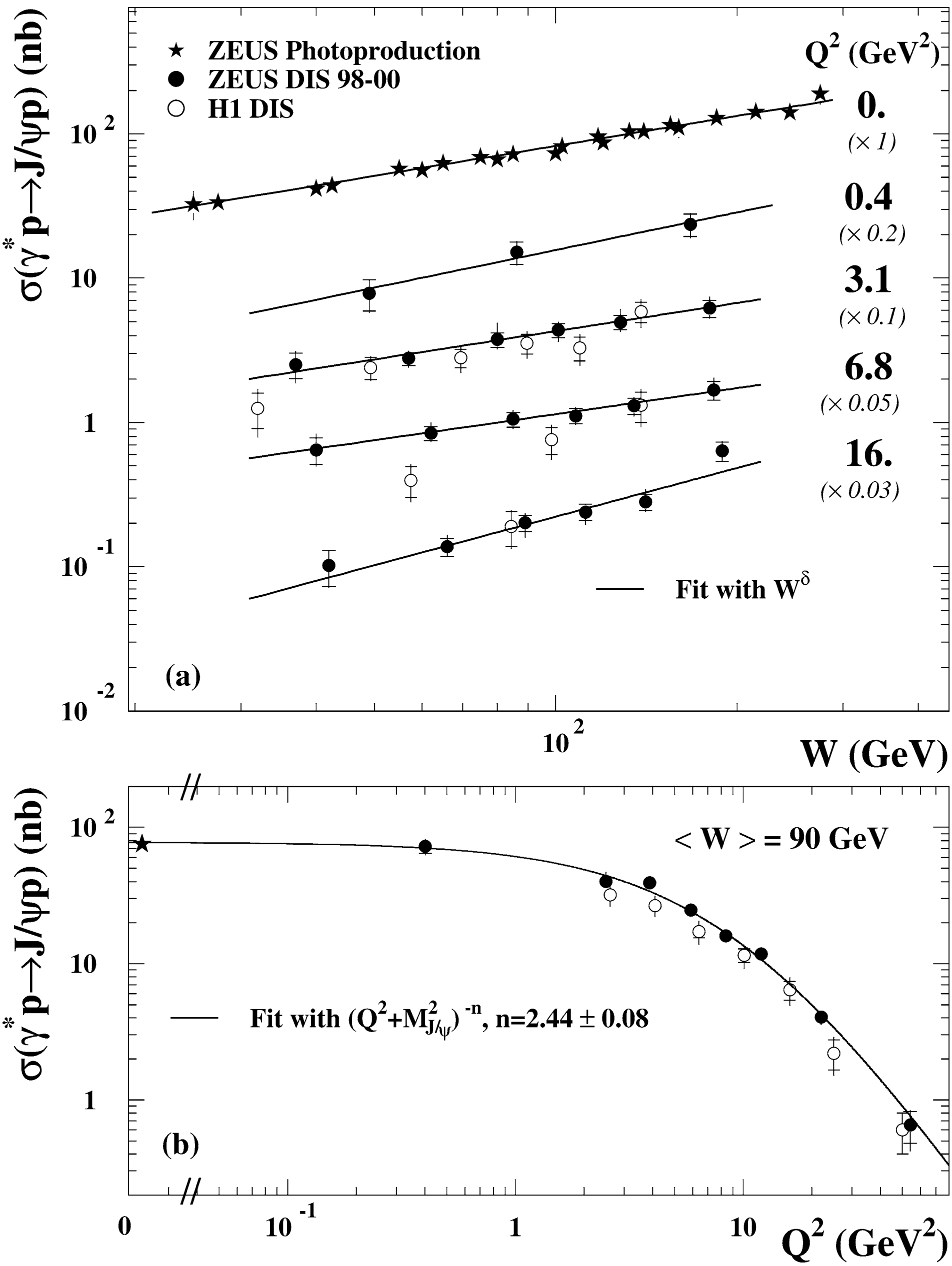

Fig. 3. Exclusive J/ψ electroproduction cross section (a) as a function of W for four values of Q^2 and (b) as a function of Q^2 at $\langle W \rangle = 90$ GeV. ZEUS photoproduction and H1 electroproduction cross sections are also shown. The full lines are fits to the ZEUS data of the form (a) $\sigma \propto W^{\delta(Q^2)}$ and (b) $\sigma \propto (Q^2 + M^2_{J/\psi})^{-n}$. The inner error bars represent the statistical uncertainties, the outer bars are the statistical and systematic uncertainties added in quadrature. An overall normalisation uncertainty of $^{+5\%}_{-8\%}$ was not included.

The function $\sigma = \sigma_0(M_{J/\psi}^2/(Q^2 + M_{J/\psi}^2))^n$, fitted to the ZEUS data including the photoproduction point, is shown in Fig. 3(b). The resulting parameters are $\sigma_0 = 77 \pm 3$ nb and $n = 2.44 \pm 0.08$, with $\chi^2/\mathrm{ndf} = 4.1/7$. The fit, which takes both the statistical and uncorrelated systematic uncertainties into account, describes the data well over the full Q^2 range.

7.3.1. Comparison to model predictions

Models based on QCD are able to describe exclusive vector meson production at HERA. In such models, in the frame where the proton is at rest, the photon emitted from the electron fluctuates into a $q\bar{q}$ state, this $q\bar{q}$ pair subsequently interacts with the proton through the exchange of gluons in a colour-singlet configuration and eventually forms a bound meson state. The transverse size of the $q\bar{q}$ pair depends on Q^2 and on the quark mass; for $Q^2 > \mathcal{O}(10)$ GeV^2 or for heavy quarks, it is assumed to be considerably smaller than the size of the proton. At such distances, the QCD coupling is small and perturbation theory can be applied. The QCD factorisation theorem for hard exclusive electroproduction of mesons [10] predicts that, in the limit of large Q^2 and fixed x, the cross section can be estimated from a hard interaction part calculable in pQCD, the $q\bar{q}$ wave function of the meson and the generalised parton distributions (GPDs) [11–13] which contain information about the correlations of the partons inside the proton and their momentum distribution. A rapid rise in the cross section with W is predicted which is related to the fast increase of the gluon density inside the proton at small values of x. Recently, NLO calculations have been completed for the exclusive photoproduction of heavy vector mesons [47]. A selection of the available models is compared to the data and discussed below. A more complete discussion on the available models is given elsewhere [14].

Frankfurt, Koepf and Strikman (FKS) [48,49] have proposed a model based on the leading-order approximation $\alpha_s \ln(Q^2)$. The usual parton distribution functions (PDFs) are used. The J/ψ wave function is estimated in the non-relativistic approximation.

In the model of Martin, Ryskin and Teubner (MRT) [50], the calculations are also performed at the leading order, $\alpha_s \ln(Q^2)$. Assuming parton–hadron duality, the component of the $c\bar{c}$ pair which has the correct spin-parity for the J/ψ is used instead of the J/ψ wave function. The cross section is integrated over the J/ψ mass range. The GPDs are estimated using the conventional next-to-leading (NLO) gluon distributions.

Gotsman et al. (GLLMN) [51] have presented a dipole model where the cross section is expressed as the convolution of the wave function of the virtual photon, the dipole scattering amplitude and the J/ψ wave function. The dipole scattering amplitude is estimated at leading order, $\alpha_s \ln(1/x)$, as the solution of the Balitsky–Kovchegov [52,53] evolution equation, including both the linear BFKL terms due to parton splitting and non-linear terms due to recombination of partons in the high-density region at low x. The J/ψ wave function is estimated in the non-relativistic approximation.

The W and Q^2 dependence of the cross sections measured by ZEUS are compared to the QCD predictions in Fig. 4. As the full NLO corrections have not yet been estimated, all the models have significant normalisation uncertainties. Therefore the normalisation was fixed using the ZEUS photoproduction data at $W = 90$ GeV; the different normalisation factors are indicated in Fig. 4. The gluon PDFs ZEUS-S [54] for MRT and CTEQ4L [55] for FKS were used. The Q^2 dependence of δ is compared in the insert in Fig. 4(a). All

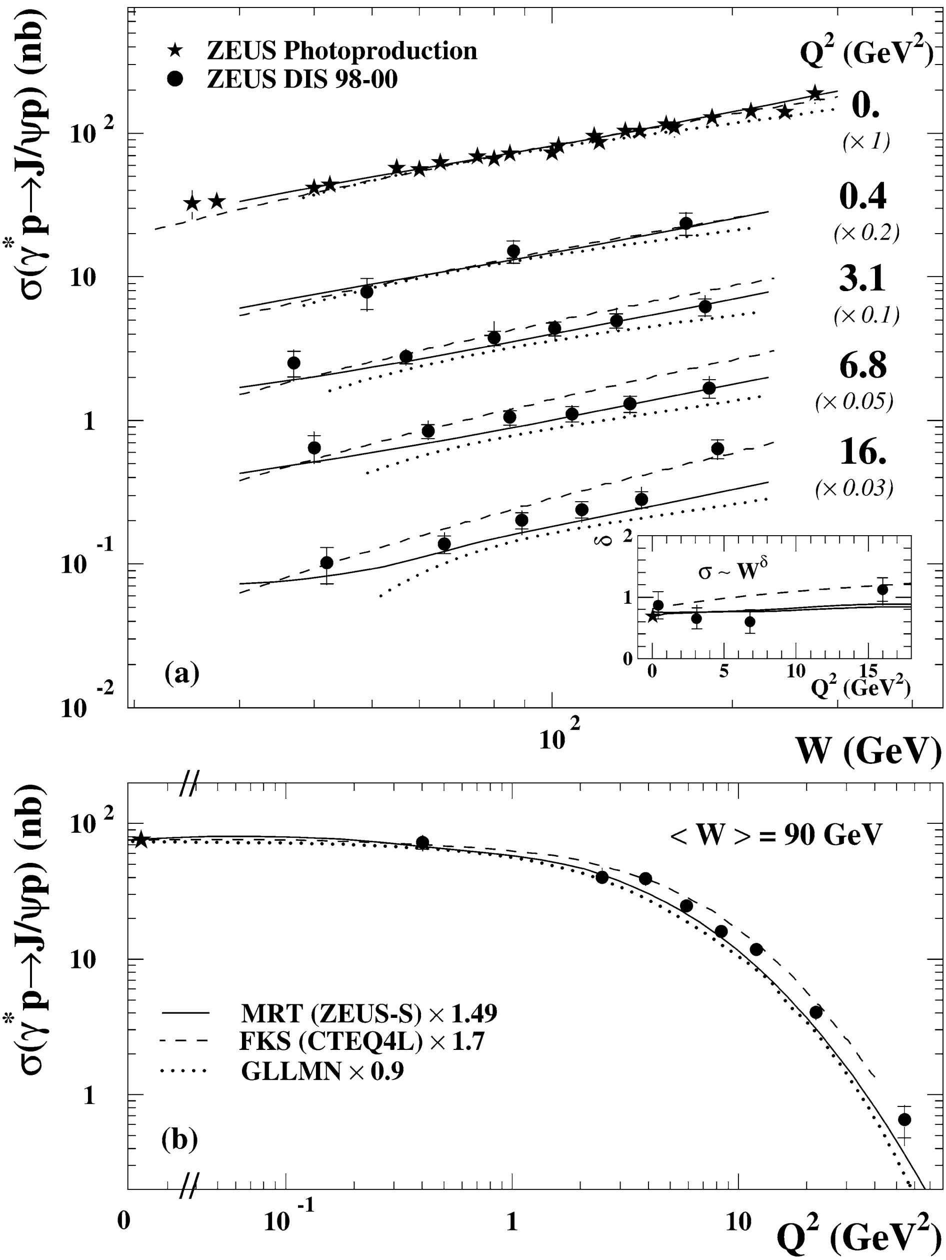

Fig. 4. Exclusive J/ψ electroproduction cross section (a) as a function of W for four values of Q^2 and (b) as a function of Q^2 at $\langle W \rangle = 90$ GeV. ZEUS photoproduction results are also shown. The curves represent the predictions of the QCD models MRT, FKS and GLLMN (see text) normalised to the ZEUS photoproduction point at $\langle W \rangle = 90$ GeV. The insert shows the parameter δ as a function of Q^2. The inner error bars represent the statistical uncertainties, the outer bars are the statistical and systematic uncertainties added in quadrature. An overall normalisation uncertainty of $^{+5\%}_{-8\%}$ was not included.

models predict a rise of the cross section with increasing W and have a Q^2 dependence similar to that of the data.

7.3.2. Comparison to model predictions for different gluon parametrisations

The MRT model was used to test three different gluon distributions: MRST02 [56], CTEQ6M [57] and ZEUS-S [54], obtained from NLO DGLAP analyses of structure function data. In deriving the GPDs from the PDFs, sensitivity to the gluon distribution at very low x is introduced. Again, the predictions were normalised to the ZEUS photoproduction measurement at $W = 90$ GeV.

Fig. 5 compares the data with the predictions. While CTEQ6M describes the W and Q^2 dependence of the data, MRST02 has the wrong shape in W, particularly at low Q^2. ZEUS-S describes the W dependence but falls too quickly with increasing Q^2.

The data exhibit a strong sensitivity to the gluon distribution in the proton. However, full NLO calculations are needed in order to use these data in global fits to constrain the gluon density.

7.4. Dependence on t

The differential cross section, $d\sigma^{\gamma^* p \to J/\psi p}/dt$, measured as a function of t in the range $|t| < 1\ \text{GeV}^2$, is shown in Table 3 and Fig. 6(a)–(d) for the high Q^2 sample as well as for three Q^2 intervals. A function of the form $d\sigma/dt = d\sigma/dt|_{t=0}\, e^{-b|t|}$ was fitted to the data and the results of the fit are given in Table 4. The slope parameter b is shown in Fig. 6(e) as a function of Q^2 and is compared to the ZEUS photoproduction and H1 electroproduction values. No significant Q^2 dependence in b is seen over the measured range of Q^2. This behaviour is different from that of exclusive ρ electroproduction, where the b slope strongly decreases with increasing Q^2, reaching the value of that of the J/ψ at $Q^2 \simeq 30\ \text{GeV}^2$ [2].

In QCD-based models, at high Q^2, the size of the $q\bar{q}$ pair in the direction transverse to the reaction axis decreases as $1/Q$ and the t dependence should reach a universal limit, independent of the flavour of the quark constituents of the meson [58]. Hence, in this limit, the t dependence is given solely by the GPDs of the nucleon. Following this idea, the differential cross section was also fitted using an elastic form factor for two-gluon exchange, $d\sigma/dt \propto (1 - t/m_{2g}^2)^{-4}$, where m_{2g}^2 is the square of the two-gluon invariant mass, as suggested by Frankfurt and Strikman [59]. The fit, including both statistical and systematic uncertainties, yields $m_{2g}^2 = 0.55 \pm 0.02\ \text{GeV}^2$ and is shown in Fig. 6(a).

7.5. Pomeron trajectory

Soft diffractive processes are described by Regge phenomenology [60] in terms of the exchange of a pomeron trajectory. In hard interactions, where Regge phenomenology may not be applicable, an effective pomeron trajectory may nevertheless be extracted. The high-Q^2 sample was analysed to determine the effective pomeron trajectory. In the Regge formalism, the differential cross section can be expressed as

$$\frac{d\sigma}{dt} \propto W^{4(\alpha_{\mathbb{P}}(t)-1)}, \tag{2}$$

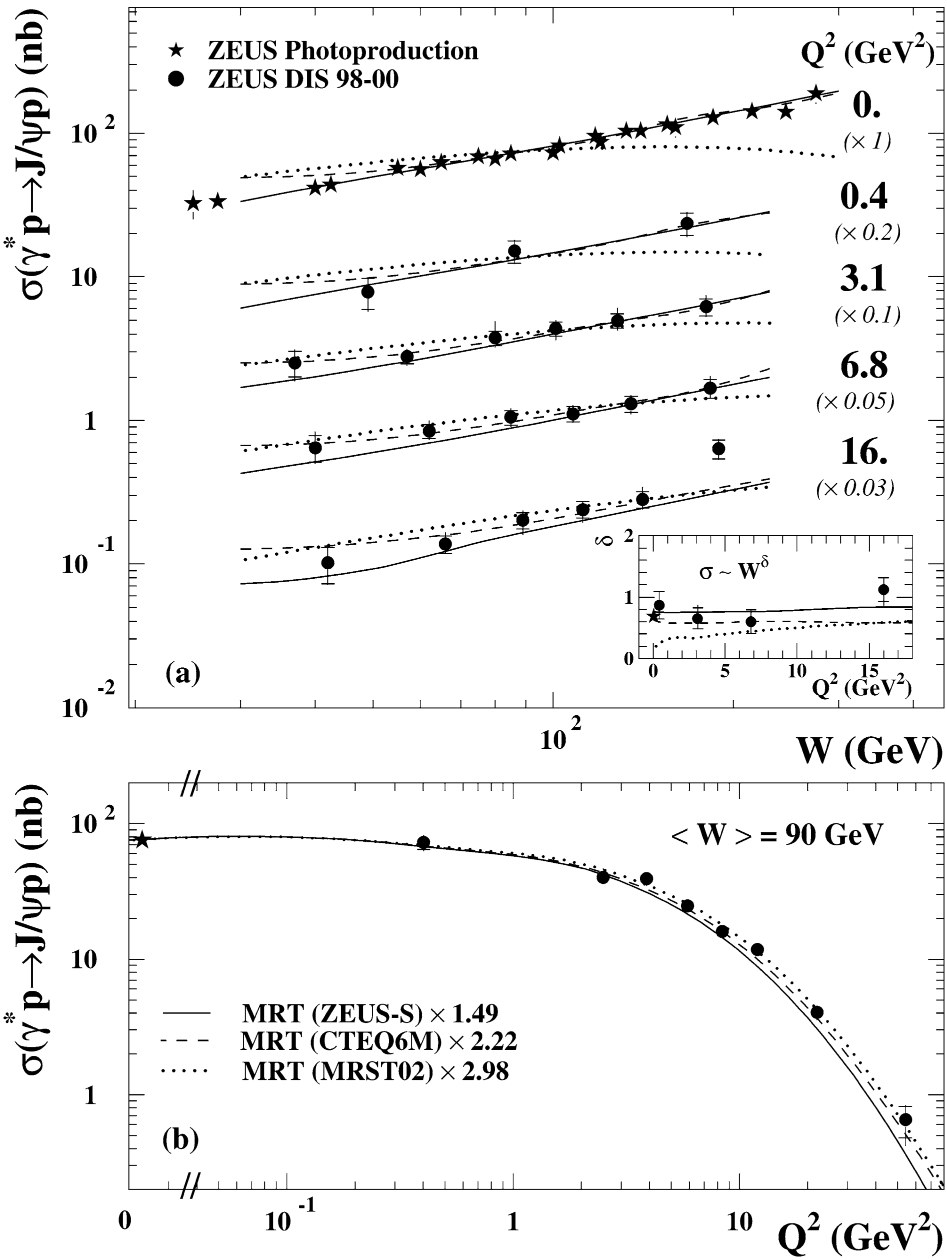

Fig. 5. Exclusive J/ψ electroproduction cross section (a) as a function of W for four values of Q^2 and (b) as a function of Q^2 at $\langle W \rangle = 90$ GeV. ZEUS photoproduction results are also shown. The data are compared to the MRT predictions (see text) obtained with different parametrisations of the gluon density and normalised to the ZEUS photoproduction point at $\langle W \rangle = 90$ GeV. The insert shows the parameter δ as a function of Q^2. The inner error bars represent the statistical uncertainties, the outer bars are the statistical and systematic uncertainties added in quadrature. An overall normalisation uncertainty of $^{+5\%}_{-8\%}$ was not included.

Table 3
The differential cross sections for the reaction $\gamma^* p \to J/\psi p$ measured as a function of t in bins of Q^2 for a mean value $W = 90$ GeV. The first uncertainty is statistical and the second systematic

Q^2 (GeV^2)	$\langle Q^2 \rangle$ (GeV^2)	$\lvert t\rvert$ (GeV^2)	$\langle \lvert t\rvert \rangle$ (GeV^2)	$d\sigma^{\gamma^* p \to J/\psi p}/dt$ (nb/GeV^2)
		0.0–0.1	0.05	$79.2 \pm 5.0^{+6.1}_{-6.5}$
2–100	6.8	0.1–0.2	0.15	$43.9 \pm 3.0^{+2.8}_{-1.9}$
		0.2–0.4	0.29	$25.8 \pm 1.4^{+1.9}_{-1.5}$
		0.4–1.0	0.58	$6.0 \pm 0.4^{+0.4}_{-0.4}$
		0.0–0.1	0.05	$148 \pm 15^{+22}_{-14}$
2–5	3.1	0.1–0.2	0.15	$86.9 \pm 9.6^{+12.5}_{-8.1}$
		0.2–0.4	0.29	$49.2 \pm 4.3^{+6.6}_{-2.8}$
		0.4–1.0	0.58	$10.7 \pm 1.1^{+0.9}_{-0.7}$
		0.0–0.1	0.05	$75.6 \pm 8.3^{+5.0}_{-9.7}$
5–10	6.8	0.1–0.2	0.15	$39.6 \pm 4.9^{+2.0}_{-2.4}$
		0.2–0.4	0.29	$23.9 \pm 2.4^{+2.1}_{-1.1}$
		0.4–1.0	0.58	$6.5 \pm 0.6^{+0.6}_{-0.3}$
		0.0–0.1	0.05	$28.0 \pm 3.4^{+2.6}_{-2.8}$
10–100	16	0.1–0.2	0.15	$15.6 \pm 2.0^{+0.9}_{-2.0}$
		0.2–0.4	0.29	$9.4 \pm 1.0^{+0.6}_{-1.4}$
		0.4–1.0	0.58	$1.8 \pm 0.2^{+0.1}_{-0.2}$

where the trajectory $\alpha_{\mathbb{P}}$ is usually parametrised as

$$\alpha_{\mathbb{P}}(t) = \alpha_{\mathbb{P}}(0) + \alpha'_{\mathbb{P}} t.$$

The effective pomeron trajectory was determined by fitting Eq. (2) to the differential cross sections at different t values. The fit was performed in four t bins at $Q^2 = 6.8$ GeV^2. Since the proton-dissociative process has the same W dependence as the exclusive process, the extraction of $\alpha_{\mathbb{P}}$ is not sensitive to this background contribution, which populates the high-t region. Therefore the analysis was extended up to $|t| = 2$ GeV^2. The fit results are shown in Fig. 7 and in Table 5. The parameters of the trajectory, determined from the linear fit are:

$$\alpha_{\mathbb{P}}(0) = 1.20 \pm 0.03(\text{stat.})^{+0.01}_{-0.02}(\text{syst.}),$$

$$\alpha'_{\mathbb{P}} = 0.07 \pm 0.05(\text{stat.})^{+0.03}_{-0.04}(\text{syst.})\ \text{GeV}^{-2}.$$

These values are in good agreement with the ZEUS results from J/ψ photoproduction [9] which are also shown in Fig. 7. They are also in agreement with expectations of pQCD-based models [61,62], but are not consistent with the trajectory measured in soft diffractive processes, $\alpha_{\mathbb{P}} = 1.08 + 0.25t$ [63,64].

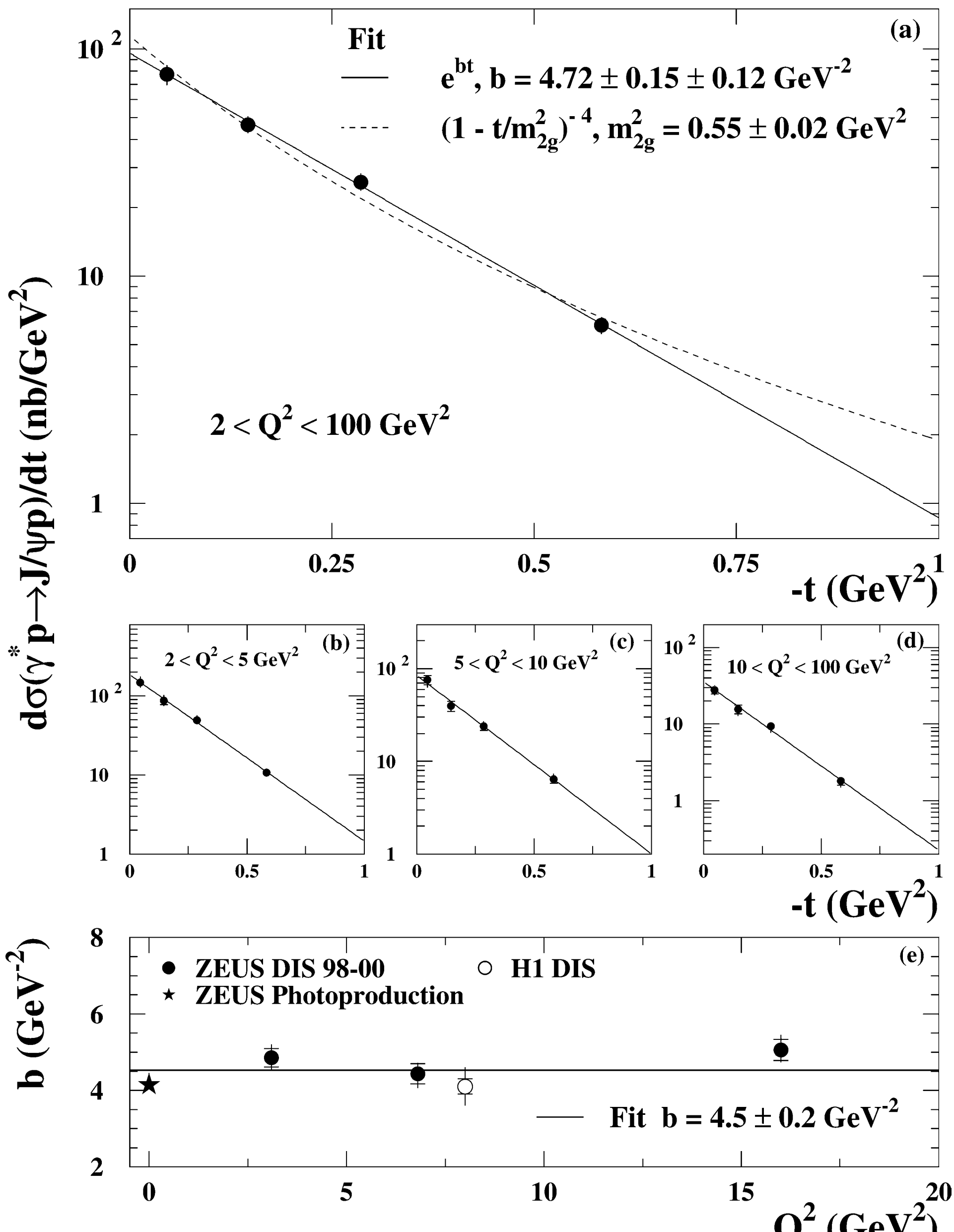

Fig. 6. Differential cross sections $d\sigma/dt$ (a) over the entire Q^2 range and (b)–(d) for three bins of Q^2, for $30 < W < 220$ GeV and $|t| < 1$ GeV^2. The full lines are the results of a fit to the form $d\sigma/dt = d\sigma/dt|_{t=0}\, e^{-b|t|}$ and the dashed line is the result of a fit using an elastic form factor assuming two-gluon exchange: $d\sigma/dt \propto (1 - t/m_{2g}^2)^{-4}$. (e) The slope b, as a function of Q^2, compared to the ZEUS photoproduction and H1 results. The mean value of b is indicated by the horizontal line. The inner error bars represent the statistical uncertainty, the outer bars the statistical and systematic uncertainties added in quadrature.

Table 4
The parameters δ, b and $\frac{d\sigma}{dt}|_{t=0}$ measured as a function of Q^2 in the range $30 < W < 220$ GeV and $45 < W < 160$ GeV for the electron and muon channels, respectively, and $|t| < 1$ GeV^2. The first uncertainty is statistical and the second systematic

Q^2 (GeV^2)	$\langle Q^2\rangle$ (GeV^2)	δ ($\sigma \propto W^\delta$)	b ($\frac{d\sigma}{dt} \propto e^{-b\|t\|}$) (GeV^{-2})	$\frac{d\sigma}{dt}\|_{t=0}$ (nb/GeV^2)
0.15–0.8	0.4	$0.87 \pm 0.22^{+0.04}_{-0.01}$		
2–5	3.1	$0.65 \pm 0.17^{+0.16}_{-0.05}$	$4.85 \pm 0.24^{+0.26}_{-0.19}$	$185 \pm 15^{+30}_{-21}$
5–10	6.8	$0.60 \pm 0.18^{+0.04}_{-0.10}$	$4.44 \pm 0.26^{+0.12}_{-0.27}$	$84.7 \pm 7.9^{+7.3}_{-9.6}$
10–100	16	$1.12 \pm 0.20^{+0.03}_{-0.16}$	$5.06 \pm 0.27^{+0.29}_{-0.17}$	$35.5 \pm 3.4^{+2.9}_{-3.5}$
2–100	6.8	$0.73 \pm 0.11^{+0.04}_{-0.08}$	$4.72 \pm 0.15^{+0.12}_{-0.12}$	$95.2 \pm 4.9^{+8.1}_{-7.9}$

7.6. Decay angular distributions

The study of the angular distributions of the decay of the J/ψ provides information about the photon and J/ψ polarisation states. In the helicity frame [65], the production and decay of the J/ψ can be described in terms of three angles (see Fig. 8): Φ_h, the angle between the J/ψ production plane and the lepton scattering plane; θ_h, the polar angle, and ϕ_h, the azimuthal angle of the positively charged decay lepton. Under the assumption of SCHC, the normalised angular distribution depends only on two angles, θ_h and $\psi_h = \phi_h - \Phi_h$, and can be expressed in the form

$$\frac{1}{N}\frac{dN}{d\cos\theta_h} = \frac{3}{8}\left[1 + r^{04}_{00} + \left(1 - 3r^{04}_{00}\right)\cos^2\theta_h\right], \tag{3}$$

$$\frac{1}{N}\frac{dN}{d\psi_h} = \frac{1}{2\pi}\left[1 - \epsilon r^{1}_{1-1}\cos 2\psi_h\right]. \tag{4}$$

The spin-density matrix element r^{04}_{00} represents the probability that the J/ψ is produced in the helicity-0 state from a virtual photon of helicity 0 or 1. The spin-density matrix element r^{1}_{1-1} gives the probability for the J/ψ to be produced in the helicity-1 state from a virtual photon of helicity 1 or -1. Assuming SCHC and natural spin-parity exchange (NPE) [65], the matrix elements r^{04}_{00} and r^{1}_{1-1} are related by

$$r^{1}_{1-1} = \frac{1}{2}\left(1 - r^{04}_{00}\right). \tag{5}$$

The cross sections at $W = 90$ GeV are shown in Fig. 9(a)–(f) for three intervals of Q^2. Eqs. (3) and (4) were fitted to the data. The values of the spin-density matrix elements r^{04}_{00} and r^{1}_{1-1}, determined from the fits, are given in Table 6. The measured values of r^{1}_{1-1} are consistent with those obtained from Eq. (5), also shown in Table 6, supporting the SCHC and NPE hypotheses.

Figs. 10 and 11 show the cross sections in bins of W and t, respectively. They are quoted at the reference value $Q^2 = 6.8$ GeV^2. Eq. (3) was fitted to the data. The values of r^{04}_{00}, given in Tables 7 and 8, are consistent with no W or t dependence.

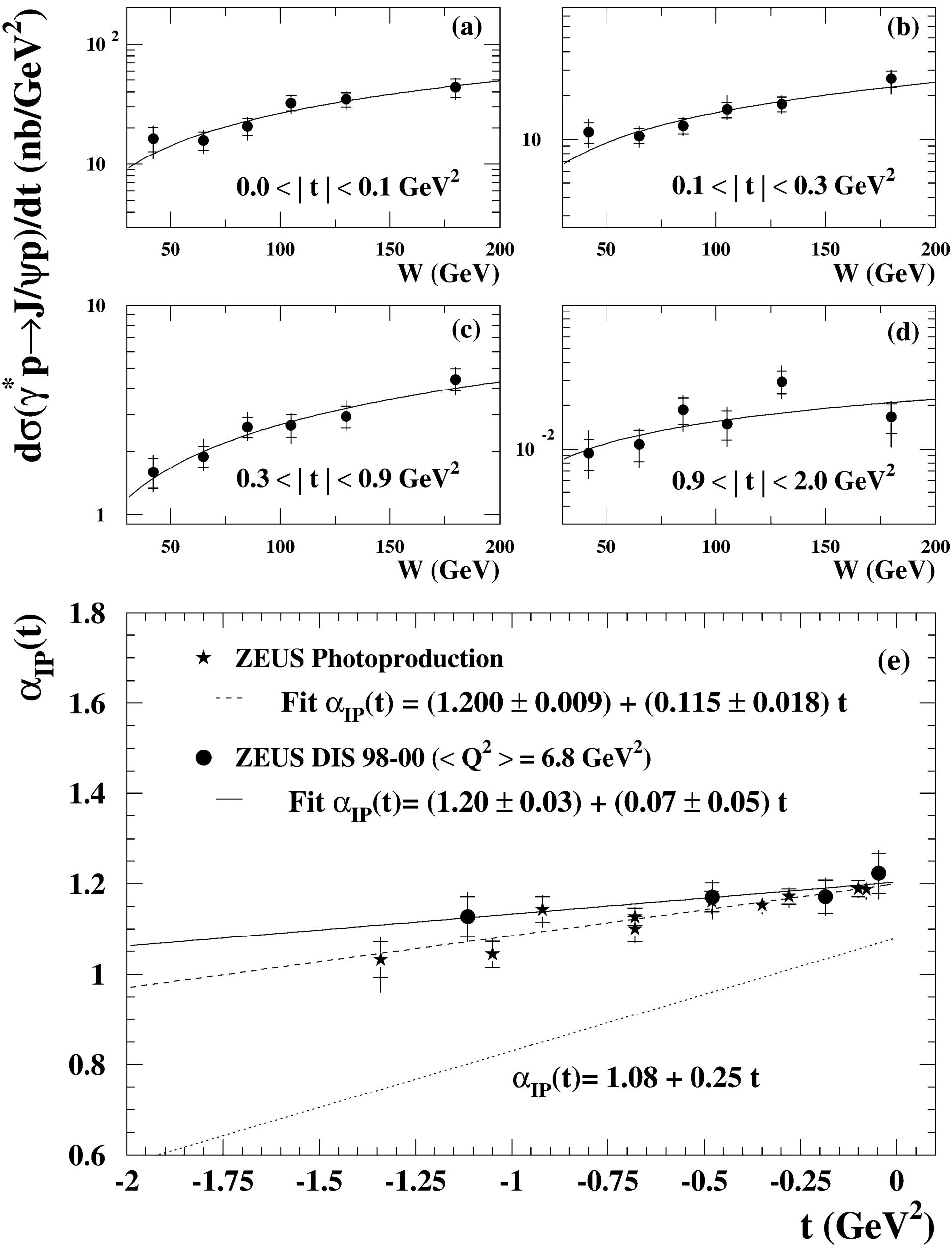

Fig. 7. (a)–(d) Differential cross sections $d\sigma/dt$ as a function of W for fixed ranges of t; the full lines are fits to $W^{4(\alpha_{\mathbb{P}}(t)-1)}$. (e) Pomeron trajectory: the lines are linear fits to the data at $\langle Q^2\rangle = 6.8\ \mathrm{GeV}^2$ (full) and to the J/ψ photoproduction results (dashed); the dotted line is the soft pomeron trajectory [66]. The inner error bars represent the statistical uncertainty, the outer bars the statistical and systematic uncertainties added in quadrature.

Table 5
The pomeron trajectory $\alpha_{\mathbb{P}}(t)$ measured in four t bins, in the range $2 < Q^2 < 100\ \text{GeV}^2$ at a mean value $\langle Q^2\rangle = 6.8\ \text{GeV}^2$. The first uncertainty is statistical and the second systematic

$\lvert t\rvert$ (GeV^2)	$\langle\lvert t\rvert\rangle$ (GeV^2)	$\alpha_{\mathbb{P}}(t)$
0.0–0.1	0.046	$1.22 \pm 0.04^{+0.03}_{-0.04}$
0.1–0.3	0.186	$1.17 \pm 0.04^{+0.02}_{-0.02}$
0.3–0.9	0.483	$1.17 \pm 0.03^{+0.02}_{-0.04}$
0.9–2.0	1.123	$1.13 \pm 0.04^{+0.03}_{-0.04}$

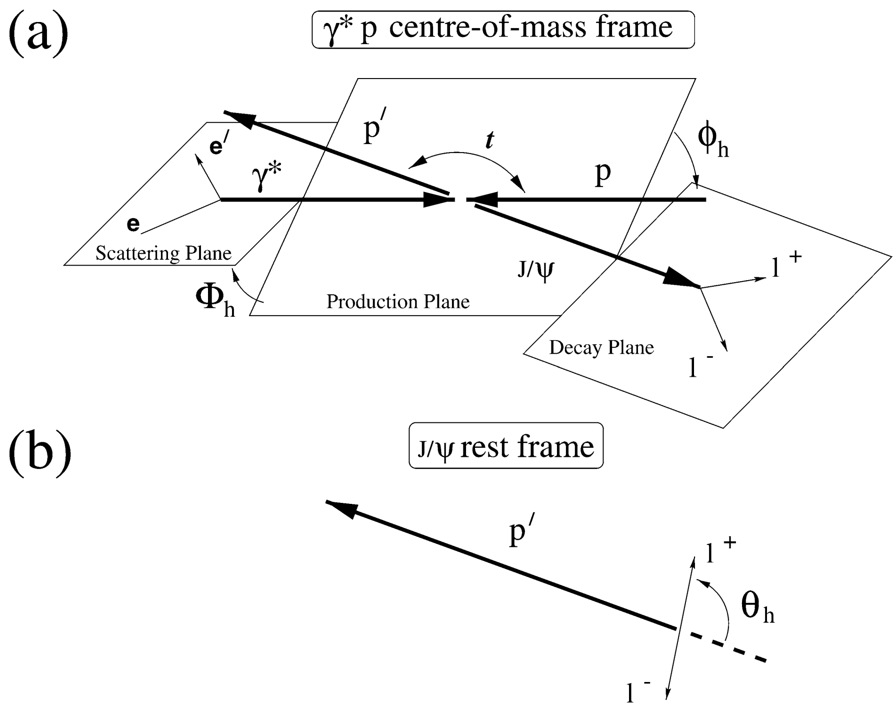

Fig. 8. Schematic diagrams of (a) the process $ep \to eJ/\psi p$ in the $\gamma^* p$ centre-of-mass system, and (b) the decay of the J/ψ in its rest frame. Three angles suffice to describe the reaction: the azimuthal angle between the scattering plane and the production plane, Φ_h; and the two J/ψ decay angles, ϕ_h, the azimuthal angle between the production and decay planes, defined in either the $\gamma^* p$ system or in the J/ψ rest frame; and θ_h, which is the polar angle of the positively-charged decay product defined with respect to the direction of the J/ψ momentum vector in the $\gamma^* p$ system, or, equivalently, the direction opposite to the momentum-vector of the final-state proton in the rest frame of the J/ψ meson. This choice of the spin-quantisation axis defines the helicity frame.

7.6.1. Longitudinal and transverse cross sections

The ratio of the longitudinal to transverse cross section, $R = \sigma_L/\sigma_T$, was calculated as a function of Q^2, W and t from r_{00}^{04} according to the relation

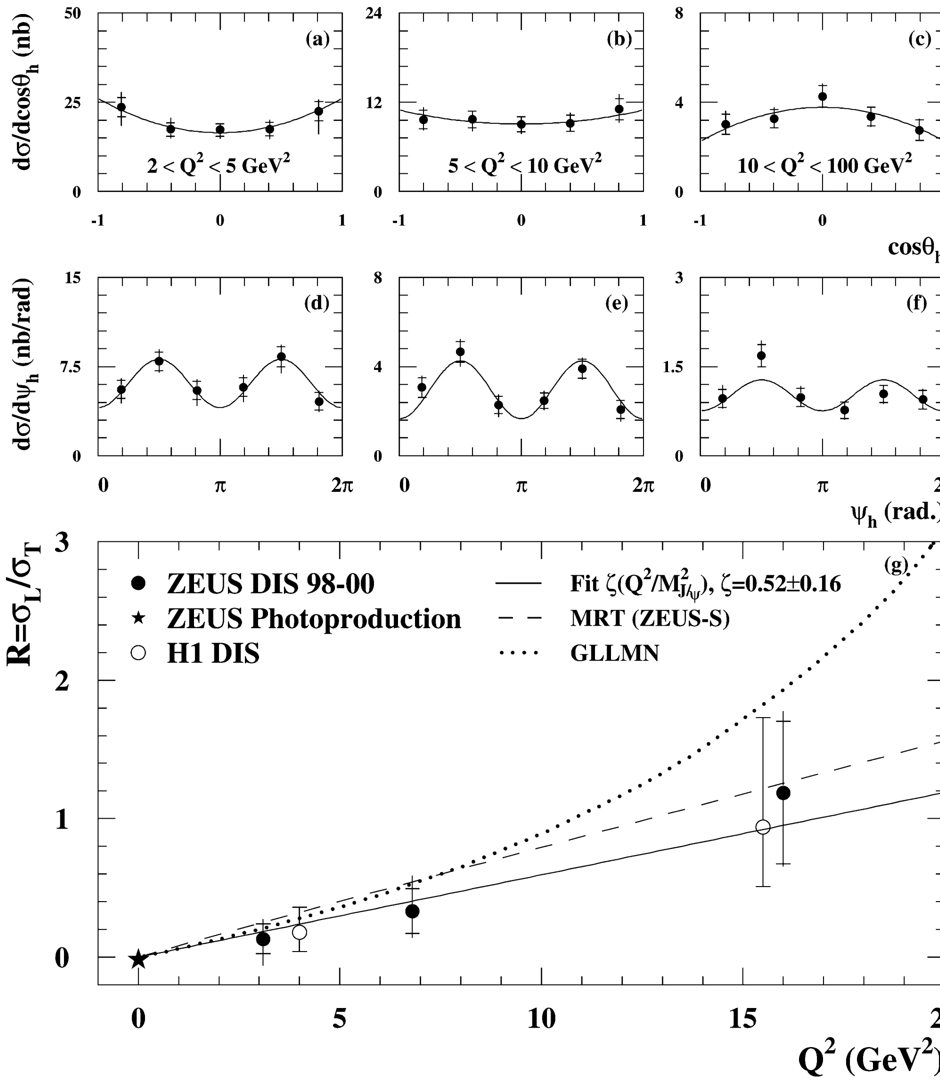

Fig. 9. (a)–(f) Distributions of $\cos\theta_h$ and Ψ_h in three Q^2 bins; the curves are the fits to Eqs. (3) and (4). (g) Ratio $R = \sigma_L/\sigma_T$ as a function of Q^2; the full curve is the result of the fit to the ZEUS data while the dashed and dotted curves are the predictions of the MRT and GLLMN models, respectively. The inner error bars represent the statistical uncertainty, the outer bars the statistical and systematic uncertainties added in quadrature.

$$R = \frac{1}{\epsilon}\frac{r_{00}^{04}}{1 - r_{00}^{04}},$$

which is valid under the assumption of SCHC.

The values of R as a function of Q^2 are given in Table 6 and compared with the H1 results [5] in Fig. 9(g). The expression $R = \zeta(Q^2/M_{J/\psi}^2)$ was fitted to the ZEUS data yielding $\zeta = 0.52 \pm 0.16(\text{stat.})$. In QCD-based models, the scale that controls the

Table 6
The spin-density matrix elements, r^{04}_{00} and r^{1}_{1-1}, the ratio of cross sections of longitudinally and transversely polarised photons, R, and the quantity $r^{1}_{1-1} - \frac{1}{2}(1 - r^{04}_{00})$ measured in bins of Q^2. The first uncertainty is statistical and the second systematic

Q^2 (GeV^2)	$\langle Q^2 \rangle$ (GeV^2)	r^{04}_{00}	r^{1}_{1-1}	$R = \sigma_L/\sigma_T$	$r^{1}_{1-1} - \frac{1}{2}(1 - r^{04}_{00})$
2–5	3.1	$0.12 \pm 0.08^{+0.13}_{-0.15}$	$0.34 \pm 0.09^{+0.03}_{-0.06}$	$0.13 \pm 0.11^{+0.09}_{-0.16}$	$-0.10 \pm 0.09^{+0.08}_{-0.06}$
5–10	6.8	$0.25 \pm 0.09^{+0.10}_{-0.06}$	$0.44 \pm 0.09^{+0.06}_{-0.07}$	$0.33 \pm 0.16^{+0.19}_{-0.11}$	$0.06 \pm 0.10^{+0.08}_{-0.06}$
10–100	16	$0.54 \pm 0.10^{+0.06}_{-0.03}$	$0.26 \pm 0.09^{+0.09}_{-0.04}$	$1.19 \pm 0.51^{+0.28}_{-0.14}$	$0.03 \pm 0.11^{+0.07}_{-0.02}$

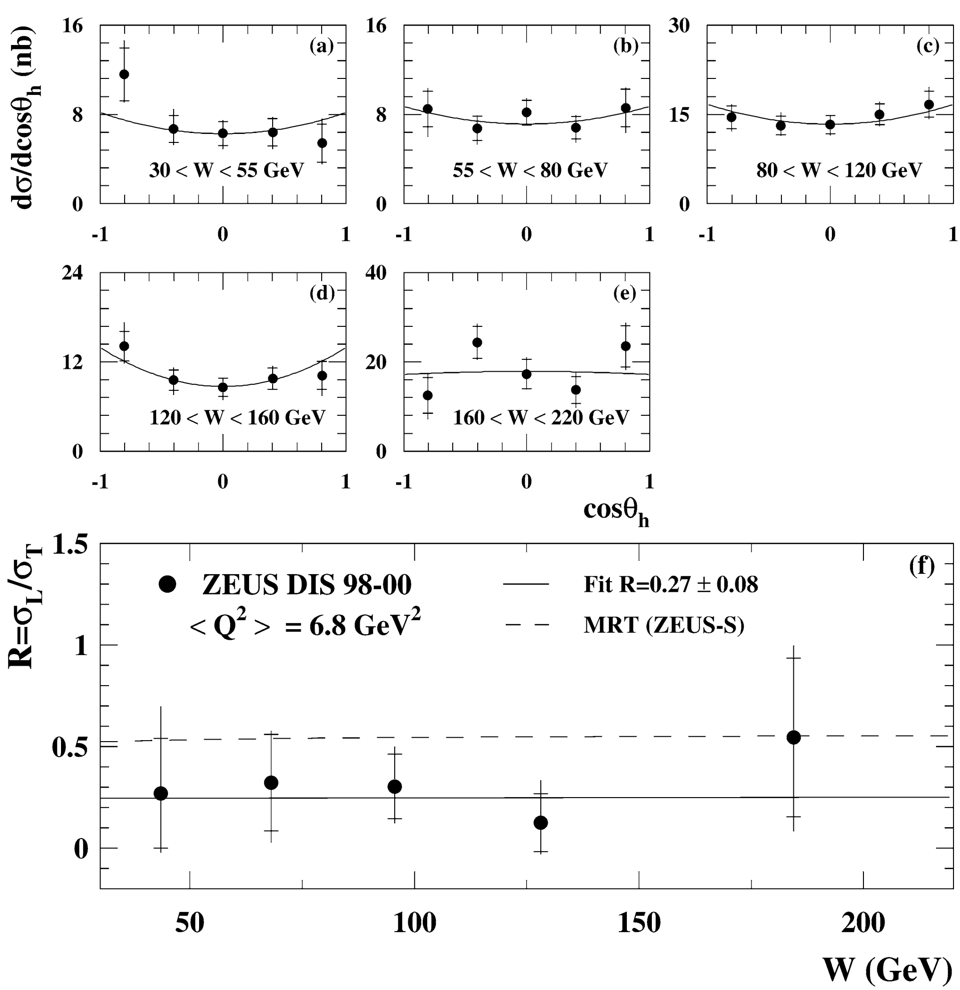

Fig. 10. (a)–(e) Distributions of $\cos\theta_h$ for five bins of W; the curves are the fits to Eq. (3). (f) Ratio $R = \sigma_L/\sigma_T$ as a function of W; the dashed line is the MRT prediction and the full line is the result of a one-parameter fit. The error bars are statistical (inner) and total (outer).

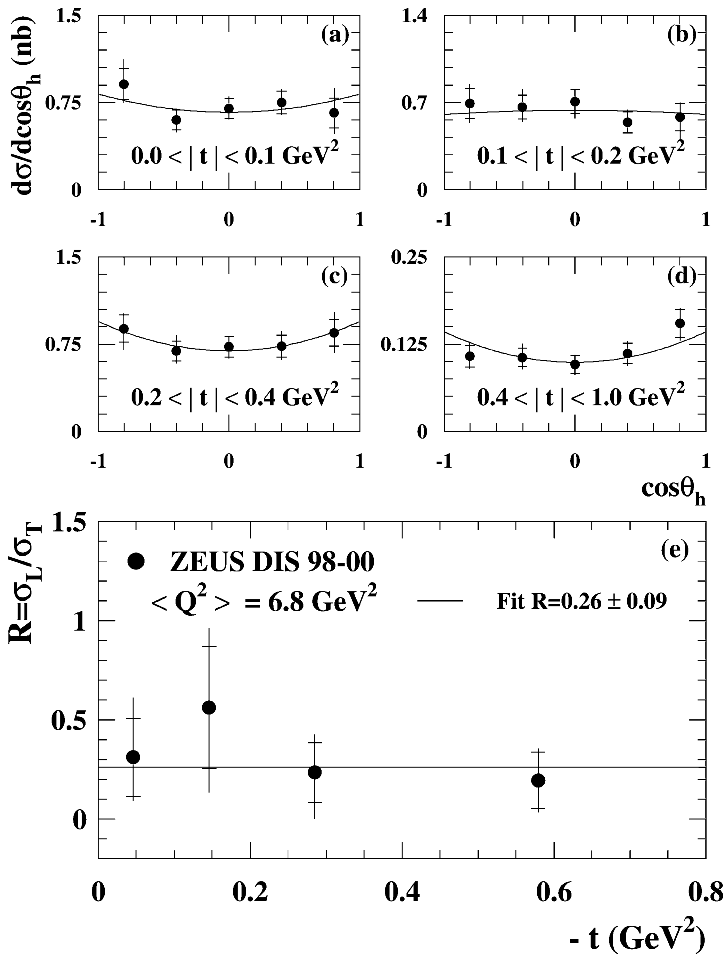

Fig. 11. (a)–(d) Distributions of $\cos\theta_h$ for four bins of t; the curves are the fits to Eq. (3). (e) Ratio $R = \sigma_L/\sigma_T$ as a function of t; the full line is the result of a one-parameter fit. The error bars are statistical (inner) and total (outer).

transverse size of the $q\bar{q}$ fluctuation of the photon may behave differently for σ_L and σ_T. However, in the MRT model, σ_L and σ_T have the same W dependence, dictated by the gluon distribution. Therefore the ratio is constant. This model correctly describes the rising behaviour of R with Q^2 whereas the GLLMN prediction somewhat overestimates it.

The values of R as a function of W and t are given in Tables 7 and 8 and shown in Figs. 10(f) and 11(g), respectively.

8. Summary

The exclusive electroproduction of J/ψ mesons, $ep \to eJ/\psi p$, has been measured with the ZEUS detector at HERA for photon virtualities in the ranges $0.15 < Q^2 < 0.8\ \text{GeV}^2$

Table 7
The spin density matrix element r_{00}^{04} and the ratio of cross sections of longitudinally and transversely polarised photons, R, measured in bins of W, in the range $2 < Q^2 < 100\ \text{GeV}^2$ at a mean value $\langle Q^2 \rangle = 6.8\ \text{GeV}^2$. The first uncertainty is statistical and the second systematic

W (GeV)	$\langle W \rangle$ (GeV)	r_{00}^{04}	$R = \sigma_L/\sigma_T$
30–55	43.5	$0.21 \pm 0.16^{+0.32}_{-0.18}$	$0.27 \pm 0.26^{+0.45}_{-0.17}$
55–80	68.1	$0.24 \pm 0.13^{+0.10}_{-0.10}$	$0.31 \pm 0.23^{+0.26}_{-0.22}$
80–120	95.6	$0.25 \pm 0.09^{+0.09}_{-0.05}$	$0.33 \pm 0.16^{+0.15}_{-0.07}$
120–160	128.1	$0.12 \pm 0.11^{+0.11}_{-0.05}$	$0.14 \pm 0.15^{+0.12}_{-0.05}$
160–220	184.4	$0.36 \pm 0.16^{+0.12}_{-0.10}$	$0.56 \pm 0.40^{+0.23}_{-0.16}$

Table 8
The spin density matrix element r_{00}^{04} and the ratio of cross sections of longitudinally and transversely polarised photons, R, measured in bins of $|t|$, in the range $2 < Q^2 < 100\ \text{GeV}^2$ at a mean value $\langle Q^2 \rangle = 6.8\ \text{GeV}^2$. The first uncertainty is statistical and the second systematic

$\lvert t \rvert$ (GeV^2)	$\langle \lvert t \rvert \rangle$ (GeV^2)	r_{00}^{04}	$R = \sigma_L/\sigma_T$
0.0–0.1	0.046	$0.24 \pm 0.11^{+0.12}_{-0.06}$	$0.31 \pm 0.19^{+0.22}_{-0.10}$
0.1–0.2	0.146	$0.36 \pm 0.13^{+0.08}_{-0.11}$	$0.56 \pm 0.30^{+0.17}_{-0.20}$
0.2–0.4	0.285	$0.19 \pm 0.10^{+0.07}_{-0.12}$	$0.23 \pm 0.15^{+0.11}_{-0.16}$
0.4–1.0	0.579	$0.16 \pm 0.10^{+0.05}_{-0.05}$	$0.19 \pm 0.14^{+0.08}_{-0.08}$

and $2 < Q^2 < 100\ \text{GeV}^2$, for photon–proton centre-of-mass energies in the range $30 < W < 220$ GeV and for four-momentum-transfer squared in the range $|t| < 1\ \text{GeV}^2$.

The cross section of the process $\gamma^* p \to J/\psi p$ rises with W as $\sigma \propto W^\delta$, with a slope parameter δ of about 0.7. This parameter does not change significantly with Q^2 and is consistent with that observed in J/ψ photoproduction.

The cross section at $W = 90$ GeV and over the whole Q^2 range is described by the function $\sigma \propto (Q^2 + M_{J/\psi}^2)^{-n}$, with $n = 2.44 \pm 0.08$.

The t distribution, measured for $|t| < 1\ \text{GeV}^2$, is well described by an exponential dependence over the range $2 < Q^2 < 100\ \text{GeV}^2$. The slope parameter, b, is consistent with being constant in this range. The mean value is $b = 4.72 \pm 0.15(\text{stat.}) \pm 0.12(\text{syst.})\ \text{GeV}^{-2}$, consistent with that observed in J/ψ photoproduction.

An analysis of the cross sections in the framework of Regge phenomenology yields an effective pomeron trajectory consistent with that measured in J/ψ photoproduction.

The spin-density matrix elements r_{1-1}^{1} and r_{00}^{04} are consistent with s-channel-helicity conservation. The ratio of the cross sections for longitudinally and transversely polarised photons, R, increases with Q^2, but is independent of W and t, within the measured range.

The J/ψ electroproduction data can be qualitatively described within the framework of pQCD that successfully describes J/ψ photoproduction data. The data exhibit a strong sensitivity to the gluon distribution in the proton. Full next-to-leading-order QCD calculations would allow these data to be used in global QCD fits to constrain the gluon density function in the proton.

Acknowledgements

We thank the DESY directorate for their strong support and encouragement. The special effort of the HERA group is gratefully acknowledged. We are grateful for the support of the DESY computing and network services. The design, construction and installation of the ZEUS detector has been made possible by the efforts and ingenuity of many people who are not listed as authors. It is a pleasure to thank E. Naftali and T. Teubner for providing us with model predictions.

References

[1] ZEUS Collaboration, J. Breitweg, et al., Eur. Phys. J. C 6 (1999) 603.
[2] H1 Collaboration, C. Adloff, et al., Eur. Phys. J. C 13 (2000) 371.
[3] H1 Collaboration, C. Adloff, et al., Phys. Lett. B 539 (2002) 25.
[4] ZEUS Collaboration, J. Breitweg, et al., Eur. Phys. J. C 12 (2000) 393.
[5] H1 Collaboration, C. Adloff, et al., Eur. Phys. J. C 10 (1999) 373.
[6] H1 Collaboration, C. Adloff, et al., Phys. Lett. B 483 (2000) 23.
[7] ZEUS Collaboration, J. Breitweg, et al., Phys. Lett. B 437 (1998) 432.
[8] H1 Collaboration, C. Adloff, et al., Phys. Lett. B 541 (2002) 251.
[9] ZEUS Collaboration, S. Chekanov, et al., Eur. Phys. J. C 24 (2002) 345.
[10] J.C. Collins, L. Frankfurt, M. Strikman, Phys. Rev. D 56 (1997) 2982.
[11] D. Muller, et al., Fortschr. Phys. 42 (1994) 101.
[12] X.D. Ji, Phys. Rev. Lett. 78 (1997) 610.
[13] A.V. Radyushkin, Phys. Rev. D 56 (1997) 5524.
[14] V. Barone, E. Predazzi, High-Energy Particle Diffraction, Springer-Verlag, Berlin, 2002, and references therein.
[15] ZEUS Collaboration, U. Holm (Ed.), The ZEUS Detector, Status Report (unpublished), DESY (1993), available on http://www-zeus.desy.de/bluebook/bluebook.html.
[16] N. Harnew, et al., Nucl. Instrum. Methods A 279 (1989) 290.
[17] B. Foster, et al., Nucl. Phys. B (Proc. Suppl.) 32 (1993) 181.
[18] B. Foster, et al., Nucl. Instrum. Methods A 338 (1994) 254.
[19] M. Derrick, et al., Nucl. Instrum. Methods A 309 (1991) 77.
[20] A. Andresen, et al., Nucl. Instrum. Methods A 309 (1991) 101.
[21] A. Caldwell, et al., Nucl. Instrum. Methods A 321 (1992) 356.
[22] A. Bernstein, et al., Nucl. Instrum. Methods A 336 (1993) 23.
[23] A. Bamberger, et al., Nucl. Instrum. Methods A 450 (2000) 235.
[24] ZEUS Collaboration, J. Breitweg, et al., Phys. Lett. B 407 (1997) 432.
[25] A. Bamberger, et al., Nucl. Instrum. Methods A 401 (1997) 63.
[26] A. Dwurazny, et al., Nucl. Instrum. Methods A 277 (1989) 176.
[27] J. Andruszkow, et al., Acta Phys. Pol. B 32 (2001) 2025.
[28] L. Hand, Phys. Rev. 129 (1963) 1834.
[29] W.H. Smith, K. Tokushuku, L.W. Wiggers, in: C. Verkerk, W. Wojcik (Eds.), Proc. Computing in High-Energy Physics (CHEP), Annecy, France, September 1992, CERN, Geneva, Switzerland, 1992, p. 222, also in preprint DESY 92-150B.
[30] W.H. Smith, et al., Nucl. Instrum. Methods A 355 (1995) 278.
[31] J. Tandler, PhD thesis, Universität Bonn, Germany, Report BONN-IR-2003-06 ISSN-0172-8741, 2003.
[32] R. Ciesielski, PhD thesis, Warsaw University, Poland, 2004.
[33] K. Voss, PhD thesis, Universität Bonn, Germany, 2004.
[34] G.M. Briskin, PhD thesis, Tel Aviv University, Report DESY-THESIS-1999-036, DESY, 1999.
[35] R. Brun, et al., GEANT3, Technical Report CERN-DD/EE/84-1, CERN, 1987.
[36] K. Muchorowski, PhD thesis, Warsaw University, Poland, 1996, unpublished.

[37] A. Kwiatkowski, H. Spiesberger, H.-J. Möhring, Comput. Phys. Commun. 69 (1992) 155;
A. Kwiatkowski, H. Spiesberger, H.-J. Möhring, in: W. Buchmüller, G. Ingelman (Eds.), Proc. Workshop Physics at HERA, vol. 3, DESY, Hamburg, 1991, p. 1419.
[38] H. Spiesberger, An Event Generator for *ep* Interactions at HERA Including Radiative Processes (Version 4.6), 1996, available on http://www.desy.de/~hspiesb/heracles.html.
[39] E. Barberio, Z. Was, Comput. Phys. Commun. 79 (1994) 291.
[40] L. Adamczyk, PhD thesis, University of Mining and Metallurgy, Cracow, Poland, Report DESY-THESIS-1999-045, DESY, 1999.
[41] M. Kasprzak, PhD thesis, Warsaw University, Warsaw, Poland, Report DESY lF35D-96-16, DESY, 1996.
[42] S.P. Baranov, et al., in: W. Buchmüller, G. Ingelman (Eds.), Proc. Workshop on Physics at HERA, vol. 3, DESY, Hamburg, Germany, 1991, p. 1478.
[43] T. Abe, Comput. Phys. Commun. 136 (2001) 126.
[44] Particle Data Group, K. Hagiwara, et al., Phys. Rev. D 66 (2002) 010001.
[45] V.M. Budnev, et al., Phys. Rep. C 15 (1974) 181.
[46] ZEUS Collaboration, S. Chekanov, et al., Eur. Phys. J. C 21 (2001) 443.
[47] D.Y. Ivanov, et al., hep-ph/0401131.
[48] L. Frankfurt, W. Koepf, M. Strikman, Phys. Rev. D 54 (1996) 3194.
[49] L. Frankfurt, W. Koepf, M. Strikman, Phys. Rev. D 57 (1998) 512.
[50] A.D. Martin, M.G. Ryskin, T. Teubner, Phys. Rev. D 62 (2000) 14022.
[51] E. Gotsman, et al., Acta Phys. Pol. B 34 (2003) 3255.
[52] I. Balitsky, Nucl. Phys. B 463 (1996) 99.
[53] Yu. Kovchegov, Phys. Rev. D 60 (2000) 034008.
[54] ZEUS Collaboration, S. Chekanov, et al., Phys. Rev. D 67 (2003) 12007.
[55] H.L. Lai, et al., Phys. Rev. D 55 (1997) 1280.
[56] A.D. Martin, et al., Eur. Phys. J. C 23 (2002) 73.
[57] J. Pumplin, et al., JHEP 0207 (2002) 012.
[58] S.J. Brodsky, et al., Phys. Rev. D 50 (1994) 3134.
[59] L. Frankfurt, M. Strikman, Phys. Rev. D 66 (2002) 031502.
[60] P.D.B. Collins, An Introduction to Regge Theory and High Energy Physics, Cambridge Univ. Press, 1977.
[61] S.J. Brodsky, et al., JETP Lett. 70 (1999) 155.
[62] L. Frankfurt, M. McDermott, M. Strikman, JHEP 0103 (2001) 45.
[63] A. Donnachie, P.V. Landshoff, Phys. Lett. B 348 (1995) 213.
[64] G.A. Jaroszkiewicz, P.V. Landshoff, Phys. Rev. D 10 (1974) 170.
[65] K. Schilling, G. Wolf, Nucl. Phys. B 61 (1973) 381.
[66] A. Donnachie, P.V. Landshoff, Nucl. Phys. B 244 (1984) 322.